Response to reviewers

We thank both reviewers for their useful comments on our paper. Please note that all line numbers refer to the version with *tracked changes*. Many of the comments below reproduce our previously uploaded responses to the reviewers' comments. This document, however, provides more detailed information about how we have modified our manuscript.

Reviewer #1

"1. Why the latitudinal bands of 30-50 are left out? It covers a considerably large area, and may be more subjective to the horizontal mixing than the polar region. Even it may be messy and don't show an as good consistency among forcing agents and across models as the polar regions or the tropical region, it still worth reporting. Furthermore, the 50S-90S may not be a good representation of the Southern Hemisphere extratropics. This is because many models suffer a too strong southern polar vortex and hence the simulated southern polar stratosphere is too isolated. This can be hinted from Fig. 4a and Fig. S4, where a clear barrier is seen near 60S."

We first note that the response of ΔSWV_{slow} to surface temperature as a function of latitude is plotted in Fig. 5a of the submitted manuscript. We also reported the regression slope of ΔSWV_{fast} vs cold point temperature fast response in Fig. 5b of the submitted manuscript.

However, to more clearly answer the reviewer's question, we have included results at 200 hPa between 30°N and 50°N in the revised supplement. Figure S1 in the revised supplement shows the equilibrium ΔSWV_{slow} and ΔSWV_{fast} and their contribution to the total equilibrium ΔSWV for water vapor averaged at 200 hPa 30°N-50°N and 30°S-50°S. Figure S2 in the revised supplement shows the slope of ΔSWV_{slow} annual mean time series vs surface temperature time series for water vapor averaged at 200 hPa 30°N-50°N and 30°S-50°S.

In the revised manuscript, we mentioned these results in lines 180-184 and lines 222-223. Our major conclusions remain the same: The slow response plays a dominant role and contributes to close to 100% of the total response for most perturbations; The sensitivity shows general agreement across different perturbations.

"2. The regression method to get the equilibrium water vapor response seems to be unnecessarily complicate, especially the results are not too different from the simple average of the last 30 years. The authors first fit the radiative flux and water vapor time series with an exponential function, then regress the last 30 years of the fitted function. All these fitting and regression have potential introduce artificial biases and uncertainties. Recent studies also show that the ECS from the Gregory method may not be a good estimate of the true ECS (e.g. Winton et al. 2020). In addition, without a sufficiently long simulation, one can not validate whether the "equilibrium" from the regression is the true equilibrium. It makes more sense to me to simply use the average of the last 30 years while acknowledging that the models have not fully reached the equilibrium."

In an early draft of this manuscript, we approximated equilibrium ΔSWV using averages of the last 30 years of the runs. However, we analyzed one model that was run for 2600 years and found that the last 30 years of a 100- or 150-year run significantly underestimated the equilibrium. Thus, we developed the method that we presently use in the paper to better produce equilibrium estimates and validated it in the 2600-year model run, which is close to its equilibrium climate state. Details of this validation are described in lines 130-140 in the revised manuscript.

However, in response to this comment, we have listed slow response estimated by averaging over the last 30 years of the coupled simulation in Table S2 of the revised supplement.

"3. It may be worth pointing out how the PDRMIP model ensembles relate to the CMIP5 ensembles. From Fig. 2b, it seems that all of these models except HadGEM3 are on the weaker side of the CMIP5 ECS estimation range. I am also surprised to see that these models do not show an more distinct efficacy among different forcing agents (Hansen et al. 2005)."

We have added a statement to the revised manuscript comparing the PDRMIP models' ECS to that in the CMIP5 ensemble in lines 64-65.

As far as forcing efficacy goes, Hansenet al. (2005) also pointed out that efficacies depend on the method of which radiative forcing is defined. A more recent paper by Richardson et al. (2019) (which we already referenced in the submitted manuscript) using PDRMIP data showed that forcing efficacies calculated from effective radiative forcing have values close to one. Our results are in good agreement with Richardson et al. (2019) (Table S3 in the revised supplement).

"4. The authors relate the slow response to the surface temperature and relate the fast response to the cold point temperature. I believe the slow response would also be regulated by the cold point temperature. It may be interesting to show that if the relationship between the stratospheric water vapor and the cold point temperature holds from the fast adjustment to the slow response."

It certainly may be the case that the slow response is mediated by TTL temperatures, but by no means is that certain. Dessler et al. (2016) showed that, in two climate models, at least, a significant fraction of the long-term trend (and slow response) was due to increases in convective moistening, which bypasses the TTL cool trap.

We have done analyses testing whether the PDRMIP models and experiments show agreement for the relation between ΔSWV_{slow} vs the CPT slow response (Figure R1 below). Results from the models and experiments show good agreement. The slope is 0.72 ppmv/K, which is larger than the slope obtained from the fast response. Nevertheless, correlation does not prove causality and this result could arise from either TTL control or if convective moistening also correlates with the CPT slow response, or some combination. We have added a sentence to the revised manuscript describing this analysis in lines 343-348.

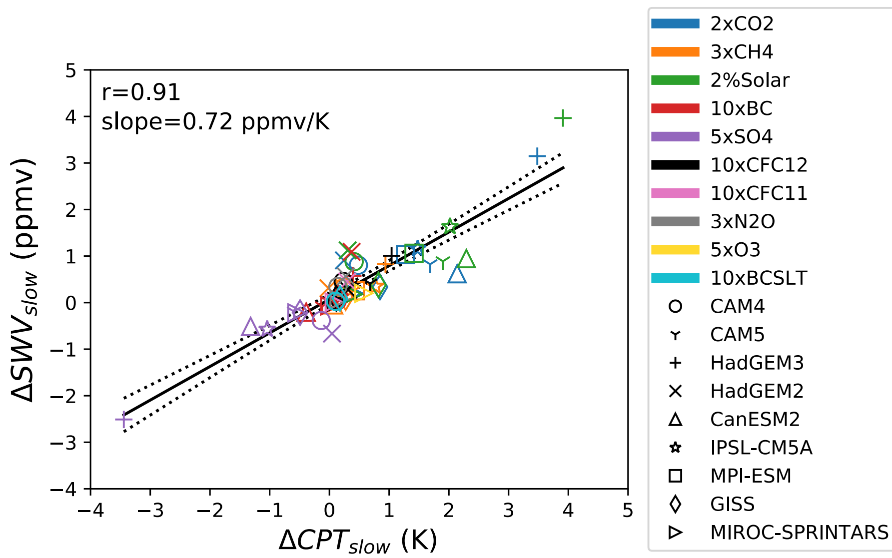

Figure R1: Same as Figure 6a of the submitted manuscript, but for TLS SWV slow response vs the CPT slow response.

"5. While Fig. 3 shows a consistent relationship between stratospheric water vapor and global mean surface temperature across various forcing, the temperature sensitivity does not seem to be so consistent in Fig. S4. Much more stratospheric moistening is seen in response to the solar forcing than others given the same surface temperature warming. This discrepancy needs to be resolved."

We list the regression slopes in the unit of ppmv/K in Table S4 and slopes in the unit of %/K in Table S5 in the revised supplement. The slope values in Table S4 are the same as we have shown in Fig. 3 of the submitted manuscript. It may not be clear in Fig. 3 of the submitted manuscript, but it is clear in Table S4 that the sensitivities are indeed larger in some experiments, such as the 2%Solar experiment. This is also the same for slopes in the unit of %/K in Table S5.

"Line 85-86: How does the averaged of fixed SST with baseline atmosphere compare to the average of the coupled baseline simulations."

For TLS SWV, the difference between fixed SST baseline simulation and coupled baseline simulation is on the order of 0.01 – 1 ppmv. For LMS SWV, the difference between fixed SST baseline simulation and coupled baseline simulation is on the order of 0.1 – 1 ppmv.

The results are averaged over the entire period of the baseline simulations for both fixed SST run and coupled run.

"Line 96: y=c+abˆx -> y=c+abˆ(-x)

We have updates this (line 119).

Line 101: Fig. S1 was not showing what is stated here. It seems the intended Fig. S1 is missing.

Line 147: Fig. S2-4. -> Fig. S1-3

Line 167: Fig. S5 -> Fig. S4"

We have updated figures and figure numbers in the supplement.

"Line 191: Does the long wave effect of the tropospheric ozone also contribute?"

Yes, the tropospheric ozone has the long wave radiative effect. We have edited the text in the revised manuscript in lines 278-280.

<u>Reviewer #2</u>

General comments

1. "The paper largely focuses on interpreting the multi-model responses. While this is of course useful, it stops short of relating the new understanding to any real-world changes in SWV... How much does this work help in understanding past and possible future SWV changes?"

"In particular, note there has been some discussion of how the PDRMIP BC perturbations compare to observations (Allan et al, https://doi.org/10.1038/s41612-019-0073-9)..."

We have added a new figure (Figure 7) and table (Table 2) and associated discussion to the paper (The "4. Historical changes in SWV" section). In this section (lines 366-400), we use our results to estimate observed changes in SWV and compare those to observations. Our estimate shows reasonable agreement with observed trend over 1980-2010.

2. "As noted in the specific comments, I feel that there is inadequate recognition that some of the results presented here are also presented, either explicitly or implicitly, in some earlier papers from the PDRMIP group – this is particularly so for the ERFs where no reference to, or comparison with, those earlier results, is given."

Thanks for pointing this out. We have added references to related results from earlier PDRMIP studies in the revised paper.

Please also see the responses to specific comments below related to previous PDRMIP studies:

"47-48: There is a slight overlap between this submitted paper and the paper published in ACP by the core PDRMIP team – Hodnebrog et al: https://doi.org/10.5194/acp-19-12887-2019, which is not cited here…"

Lines 53-55, 94-95, 374-375.

"129: I think it is necessary that a comparison of ERFs (and the associated feedback parameter) with Richardson et al. (including for the CFCs and N2O in their supplement) is presented both to confirm they are in reasonable agreement and also to make clear that the ERFs derived here are not original work with the PDRMIP output."

We have added a Table S3 in the revised supplement comparing our ERFs with "ERF_{sst}" from Richardson et al. (2019). The comparison shows good agreement. Texts mentioning this comparison are in lines 151-158 of the revised manuscript.

Specific comments

"14: This conclusion is specific to the TLS"

Yes, we agree with this, although the cold point temperature does have *some* influence in the lowermost SWV (Dessler et al., 1995). But the control is not as strong as that in the TLS (see Fig. 6b-c in submitted manuscript) and the lowermost SWV is controlled by multiple factors. We have edited the text to make this clearer (lines 13-14).

"16: "becomes weaker at higher altitudes and at higher latitudes below 150 hPa." This is a bit ambiguous. Does this means heights at pressures below 150 hPa or heights below the height of the 150 hPa surface. These would have opposite meanings."

It means altitudes below the 150 hPa surface. We have edited the text for clarity (line 16).

"57: Presumably the 3xCH4 experiments have no resulting change in SWV due to the oxidation of additional methane?"

Yes, indirect chemical effects are not included in the $3xCH_4$ experiment. We have added a sentence saying this (line 77-78).

"90 and many other places: There are repeated statements that there is no surface temperature response in the fixed SST runs, but this is not correct, with implications for the definition of ERF."

Yes, the reviewer is correct that land surface temperatures can respond to the forcing. We have edited the text in the revised manuscript (lines 108-110).

"139: tend to be larger" Isn't it clearly larger?

Yes, the reviewer is correct. We have edited this text in the revised manuscript (line 175).

*"*148 and throughout: Rather little is said about intermodel differences. For example, on HADGEM3, more discussion of its apparent outlier status on some plots seems necessary. The text says it is "likely connected" to the larger surface warming, but it seems the climate sensitivity is about double the multi-model average but the slow SW response is around a factor of 4 larger. Is that because the TTL temperature change is 4 times higher (per unit ERF)?"*

To answer the question about the HadGEM3 model, Figure R2 below shows the equilibrium slow response of TTL temperature (ΔT_{slow}) per unit ERF. The HadGEM3 ΔT_{slow}/ERF is between 2.64-3.97 times the multi-model mean ΔT_{slow}/ERF for experiments 2xCO_2, 3xCH_4, 2%Solar, 10xBC, and 10xCFC-12. Since the surface warming in HadGEM3 is larger than all other models, its upper tropospheric warming is also largest. Longwave radiation emitted from the upper troposphere warms the TTL level (Lin et al., 2017), so the larger upper tropospheric warming in HadGEM3 also results in larger TTL heating than other models. The relationship between surface warming and TTL warming is not linear.

That said, we cannot conclusively identify a cause given the information archived. So we have removed the claim that the difference is likely connected to surface warming and we have added a sentence saying more work on the causes of these differences is warranted (lines 189-190).

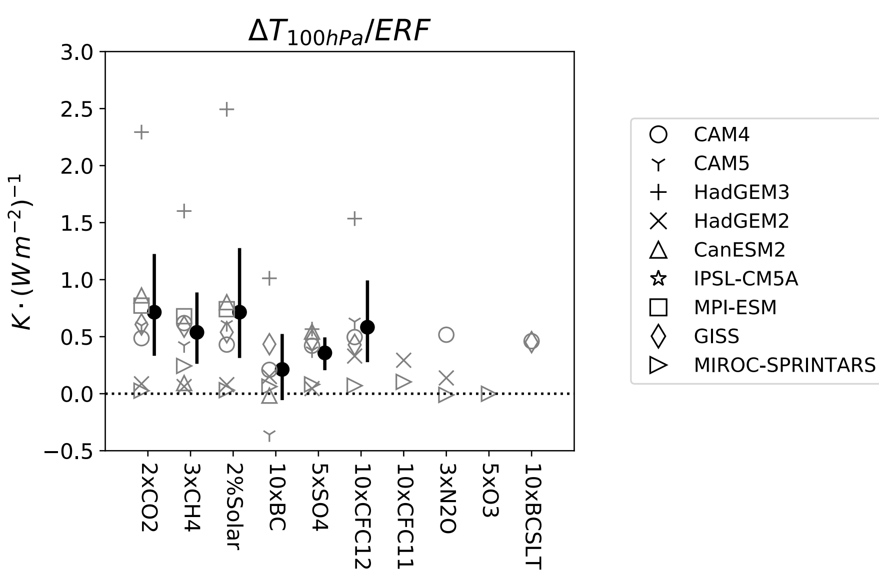

Figure R2: Equilibrium slow response of TTL temperature (100 hPa, averaged between 30°N-30°S) per ERF for all models and perturbations.

"Another example is that apparently half the models have a slow SW response to BC of the opposite sign (Fig 1a) to the multi-model mean. Is there any obvious reason why? As far as I can see BC causes a warming in all models."

Figure R4 below shows the vertical profile of tropical temperature slow (a) and fast (b) responses per unit ERF for the 10xBC experiment. The 10xBC does cause a warming at the surface and in the troposphere due to a positive TOA ERF in all models. In the TTL and lower stratosphere (LS), however, the heating is mainly caused by the fast adjustment (Fig. R3b below). The slow temperature response in the TTL is the residual of the total response minus the fast adjustment, which is negative or close to zero (Fig. R3a below).

It is therefore our contention that some of these negative values are artifacts of the method we use to estimate equilibrium response. Support for this comes from Fig. 3 of the paper. The values in this figure come from regressions of ΔSWV_{slow} vs. ΔTs in the BC runs. This method does not require differencing two large numbers, so we feel it is more robust. It shows that most models have a positive response of SWV due to BC-induced warming. For those models that produce negative slopes for ΔSWV_{slow} vs. ΔTs in the BC runs, there is large uncertainty in the regression, because the surface temperature change in those models are small.

We have noted this explanation in the revised manuscript (lines 191-196).

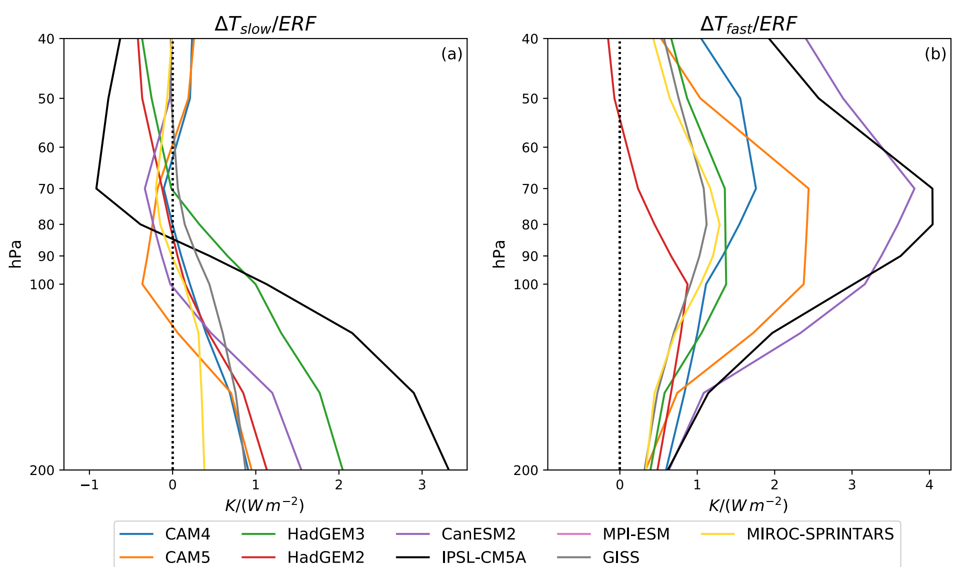

Figure R3: Profiles of equilibrium slow (a) and fast (b) temperature response for the 10xBC experiment, normalized by ERF ($K\cdot(Wm^{-2})^{-1}$), and averaged over 30°N-30°S. The color coding indicates results from different models.

"One thing I miss from this study, and encourage the authors to look at if they have the resource, is the degree to which the model's background climatology of stratospheric water vapor or TTL temperature could explain some of the intermodel differences."

We have investigated the SWV in the fixed SST baseline simulations. Based on our analyses, the baseline climatology SWV does not explain the inter-model differences in the responses to forcing agents. As an example, Fig. R4 below shows the TLS SWV slow response (first row) and TTL temperature slow response (second row) vs. the baseline TLS SWV climatology and baseline TTL temperature climatology. We omitted $3xN_2O$, $5xO_3$, and 10xBCSLT, because fewer than three models performed these experiments. There is no correlation between the SWV and temperature slow responses and the baseline climatology. In particular, HadGEM3 produces extremely large slow responses for most experiments, however, in Fig. R4 below, its baseline SWV and temperature climatology is not the largest among the models.

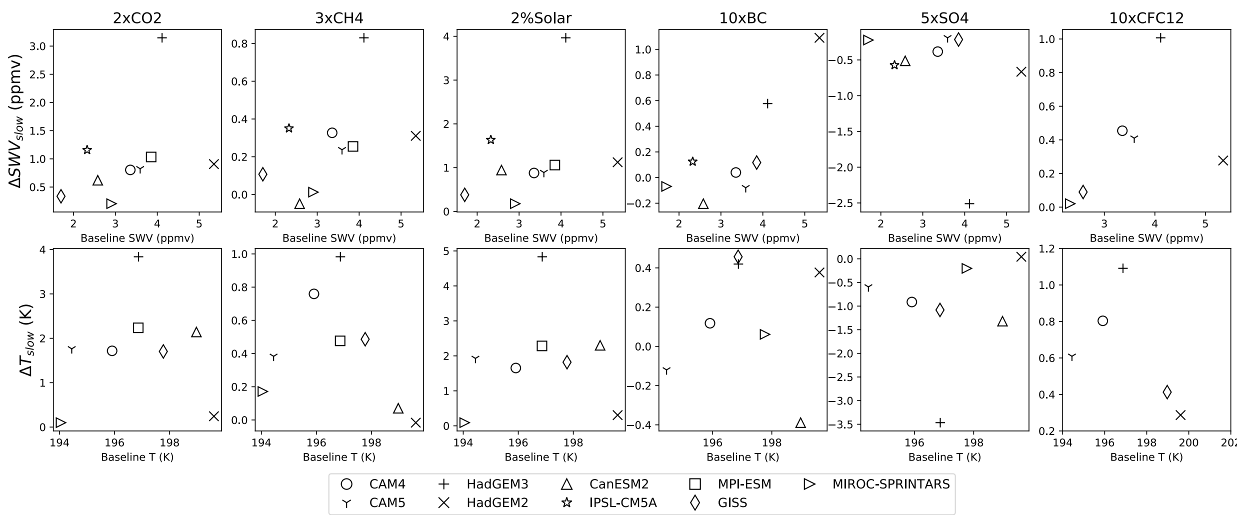

Figure R4: Top row: The TLS SWV slow response (ppmv) vs. the baseline TLS SWV climatology (ppmv). Bottom row: The TTL temperature slow response (K) (100 hPa, averaged over 30°N-30°S) vs. the baseline TTL temperature climatology (K) (100 hPa, averaged over 30°N-30°S). The baseline climatology is obtained from the fixed SST simulations averaged over the last 10 years.

"156: Is this linear regression done once across all simulations and all perturbations. If not, I am unclear which perturbations have been used for the regression."

We have added a sentence "We do this regression for each model and perturbation separately" to avoid confusion (lines 202-203).

"159: This is a relatively short paper and I wondered whether the supplementary figures could be brought into the main text?"

It remains our opinion that the key figures are included in the paper. Thus, in order to keep the take-home message concise, we have left the content of the supplement unchanged.

"171-172: This repeats a point already made at 141-142."

We'll have removed the repeated text.

"201: I am sorry if I miss it, but I see very little discussion of stratospheric temperature changes in the Jain et al paper. The role of CFCs on the vertical profile of temperature can be seen in many papers such as Forster et al. https://doi.org/10.1007/s003820050182 and Forster and Joshi 10.1007/s10584-005- 5955-7…"

In the submitted paper where we discussed the radiative heating in the UTLS by CFCs, we were referring to the text in Section 3.3 of (Jain et al., 2000), where they stated that "Halocarbons absorb predominantly in the window region (750-1250 cm^{-1}), in the linear line limit; therefore in the stratosphere they absorb the upwelling radiation from the troposphere and increase the heating rate of the stratosphere".

We agree with the reviewer that it is useful to reference papers that explicitly investigated vertical temperature profiles forced by CFCs. We have added these references in the revised manuscript (line 272).

*"*204: This statement on shortwave radiation is strange. There may be a small shortwave effect from the reduced reflected flux from the troposphere, but there is a long history of simulations that clearly attribute the stratospheric cooling due to increased tropospheric ozone to the decreased upwelling thermal infrared radiation. E.g. Ramaswamy and Bowen https://doi.org/10.1029/94JD01310, Berntsen et al https://doi.org/10.1029/97JD02226 and the Forster et al. paper referred to above."*

Thanks for pointing this out. We have edited the text to say, "Increases of tropospheric O_3 ($5xO_3$) reduce the upwelling longwave radiation, which cools the stratosphere. The longwave radiation absorbed heat the TTL region" (lines 278-280). References are also added in lines 278-280.

"206: "Tropospheric O3 is also transported". As I understand it, ozone is imposed in the models and not advected. I don't know what this sentence means."

This is correct: In the $5xO_3$ experiment, the PDRMIP group used 5 times the tropospheric ozone distribution (TROP) in the paper by MacIntosh et al. (2016) (line 76). We have removed the text about transport.

"212: "larger than 50%". CAM5 and MPI-ESM look less than 50%?"

Yes, this was poorly worded. We have completely re-written the paragraph in lines 274-277.

*"*248: Returning to General Point#1, the Summary feels a very mechanical repetition of the results in the paper without any discussion of the wider implications, remaining uncertainties, or possible future avenues/priorities for improving understanding."*

We added our discussion on wider implications and remaining uncertainties to "4. Historical changes in SWV" section in the revised manuscript (lines 366-400).

"273: Strictly Fig 5 refers to TLS only"

We have edited the text (line 427).

"519-520: I think the markers are only reported when there are more than 3 contributing models?"

Yes, the multi-model mean and error bars are shown for perturbations that are performed by more than three models. We have added this caveat to the revised figure captions.

"46L "responses" -> "responds""

We have modified the text (line 53).

"Throughout: This may be common usage, but the paper refers throughout to the ensemble mean when other papers would refer to it as the multi-model mean (ensemble could refer to different runs from the same model with perturbed initial conditions or physics…"

Thanks for pointing this out. To avoid confusion, we have replaced the "ensemble mean" with multi-model mean in the revised manuscript.

References

Dessler, A. E., Hintsa, E. J., Weinstock, E. M., Anderson, J. G. and Chan, K. R.: Mechanisms controlling water vapor in the lower stratosphere: "A tale of two stratospheres," J. Geophys. Res., 100(D11), 23167, doi:10.1029/95JD02455, 1995.

Dessler, A. E., Ye, H., Wang, T., Schoeberl, M. R., Oman, L. D., Douglass, A. R., Butler, A. H., Rosenlof, K. H., Davis, S. M. and Portmann, R. W.: Transport of ice into the stratosphere and the humidification of the stratosphere over the 21st century, Geophys. Res. Lett., 43(5), 2323–2329, doi:10.1002/2016GL067991, 2016.

Hansen, J.: Efficacy of climate forcings, J. Geophys. Res., 110(D18), D18104, doi:10.1029/2005JD005776, 2005.

Jain, A. K., Briegleb, B. P., Minschwaner, K. and Wuebbles, D. J.: Radiative forcings and global warming potentials of 39 greenhouse gases, J. Geophys. Res. Atmos., 105(D16), 20773–20790, doi:10.1029/2000JD900241, 2000.

Lin, P., Paynter, D., Ming, Y. and Ramaswamy, V.: Changes of the Tropical Tropopause Layer under Global Warming, J. Clim., 30(4), 1245–1258, doi:10.1175/JCLI-D-16-0457.1, 2017.

MacIntosh, C. R., Allan, R. P., Baker, L. H., Bellouin, N., Collins, W., Mousavi, Z. and Shine, K. P.: Contrasting fast precipitation responses to tropospheric and stratospheric ozone forcing, Geophys. Res. Lett., 43(3), 1263–1271, doi:10.1002/2015GL067231, 2016.

Richardson, T. B., Forster, P. M., Smith, C. J., Maycock, A. C., Wood, T., Andrews, T., Boucher, O., Faluvegi, G., Fläschner, D., Hodnebrog, Ø., Kasoar, M., Kirkevåg, A., Lamarque, J. -F., Mülmenstädt, J., Myhre, G., Olivié, D., Portmann, R. W., Samset, B. H., Shawki, D., Shindell, D., Stier, P., Takemura, T., Voulgarakis, A. and Watson-Parris, D.: Efficacy of Climate Forcings in PDRMIP Models, J. Geophys. Res. Atmos., 124(23), 12824–12844, doi:10.1029/2019JD030581, 2019.

The response of stratospheric water vapor to climate change driven by different forcing agents

Xun Wang[1] and Andrew E. Dessler[1]

[1]Department of Atmospheric Sciences, Texas A&M University, College Station, TX, USA

Correspondence to: Andrew E. Dessler (adessler@tamu.edu)

Abstract. We investigate the response of stratospheric water vapor (SWV) to different forcing agents within the Precipitation Driver and Response Model Intercomparison Project (PDRMIP) framework. For each model and forcing agent, we break the SWV response into a slow response, which is coupled to surface temperature changes, and a fast response, which is the response to external forcing, but before the sea surface temperatures have responded. Our results show that, for most climate perturbations, the slow SWV response dominates the fast response. The slow SWV response exhibits a similar sensitivity to surface temperature across all climate perturbations. Specifically, the sensitivity is 0.35 ppmv K^{-1} in the tropical lower stratosphere (TLS), 2.1 ppmv K^{-1} in the northern hemispheric lowermost stratosphere (LMS), and 0.97 ppmv K^{-1} in the southern hemispheric LMS. In the TLS, the fast SWV response only dominates the slow SWV response when the forcing agent radiatively heats the cold point region — for example, black carbon, which directly heats the atmosphere by absorbing solar radiation. The fast SWV response in the TLS is primarily controlled by the fast adjustment of cold point temperature across all climate perturbations. This control becomes weaker at higher altitudes in the tropics and altitudes below 150 hPa in the LMS.

Deleted: SWV

Deleted: direct

Deleted: without any mediation from

Deleted: temperature

Deleted: The

Deleted: at higher latitudes

1 Introduction

Stratospheric water vapor plays an important role in global climate change. It is an important greenhouse gas (GHG), which affects the Earth's radiative budget (Forster and Shine, 2002; Solomon et al., 2010), and it also plays an important role in stratospheric ozone chemistry (Solomon et al., 1986; Dvortsov and Solomon, 2001).

SWV in the overworld (above 380-K isentropic surface) (e.g. Hoskins, 1991) and SWV in the extratropical lowermost stratosphere (LMS, between the extratropical tropopause and the 380-K isentropic surface) (e.g. Holton et al., 1995) are distinguished according to different mechanisms that control them. Overworld SWV is primarily controlled by the temperatures in the tropical tropopause layer (TTL) as air is transported through it (e.g. Mote et al., 1996; Fueglistaler et al., 2009) and by production from oxidation of methane (e.g. Brasseur and Solomon, 2005). The LMS SWV is controlled by three major sources, including the transport of overworld air by the downward branch of Brewer-Dobson circulation, adiabatic quasi-horizontal transport from the tropical upper troposphere, and diabatic cross-tropopause transport due to deep convection (Dessler et al., 1995; Holton et al., 1995; Plumb, 2002; Gettelman et al., 2011).

The response of SWV to climate change can be partitioned into two components: the fast response and slow response. The addition of a radiatively active constituent to the atmosphere can influence the atmosphere even before the surface temperature changes, leading to changes in SWV. This is often referred to as an “adjustment” to the forcing, and is generally considered part of the external forcing (e.g. Sherwood et al., 2015). We will refer to this as the “fast response” of SWV to the forcing. The slow response is the component in the SWV change that is coupled to changes of the surface temperature, which occurs on longer time scales. This slow response means that SWV could be an important positive feedback to global warming (Forster and Shine, 2002; Dessler et al., 2013; Huang et al., 2016; Banerjee et al., 2019). Banerjee et al. (2019) have shown that, when CO_2 is abruptly quadrupled, the change in SWV mainly consists of the slow response and that the fast response is less important.

Previous studies have shown that climate models, which are able to accurately reproduce observed interannual variations in SWV (Dessler et al., 2013; Smalley et al., 2017), robustly project a positive long-term trend in overworld SWV at entry level with a warming climate due to increasing GHGs (Gettelman et al., 2010; Dessler et al., 2013; Smalley et al., 2017). This is mainly due to a warmer tropopause (Thuburn and Craig, 2002; Gettelman et al., 2010; Lin et al., 2017; Smalley et al., 2017; Xia et al., 2019), which is controlled, to some extent at least, by the warming surface (Gettelman et al., 2010; Shu et al., 2011; Dessler et al., 2013; Huang et al., 2016; Revell et al., 2016; Lin et al., 2017; Smalley et al., 2017; Banerjee et al., 2019). Dessler et al. (2016) suggested that increases in convective injection into the stratosphere due to a warming climate may also be contributing to the trend in entry SWV. In the LMS, the climate models show larger increases in SWV (Dessler et al., 2013; Huang et al., 2016; Banerjee et al., 2019). It is not known how SWV responds to different forcing agents. Hodnebrog et al. (2019) investigated the response of global integrated water vapor to different forcing agents, but focused on the troposphere.

Deleted: Dessler et al. (2016)

Deleted: It is not known how SWV responses to different forcing agents

The goal of this study is to investigate the response of both overworld and LMS SWV to forcing agents with different physical properties. We will explicitly investigate the fast and slow responses in SWV and compare them. We will also investigate how SWV responds to surface temperature change when the climate is forced by different forcing agents.

2. Method

2.1 The PDRMIP set-up

In this paper, we analyze nine models from the Precipitation Driver and Response Model Intercomparison Project (PDRMIP) (Samset et al., 2016; Myhre et al., 2017; Tang et al., 2018, 2019). These are Coupled Model Inter-comparison Project phase 5 (CMIP5) era models (Table 1) and each performed a baseline and multiple climate perturbation experiments (Table 1).

This subset of the CMIP5 ensemble has a multi-model mean equilibrium climate system (ECS) of 3.6 K, close to the ensemble-average ECS of the entire CMIP5 ensemble (3.3 K) (Zelinka et al. 2020).

In the perturbation experiments, perturbations on a global scale are applied abruptly at the beginning of the model simulation. The five core experiments include a doubling of CO_2 concentration ($2xCO_2$), a tripling of CH_4 concentration ($3xCH_4$), a 2% increase in solar irradiance (2%Solar), an increase of present-day black carbon concentration or emission by factor of 10 (10xBC), and an increase of present-day SO_4 concentration or emission by factor of 5 ($5xSO_4$). In addition to the five core experiments, a subset of models also performed additional perturbation experiments: an increase in CFC-11 concentration from 535 ppt to 5 ppb (hereafter, 10xCFC-11), an increase in CFC-12 concentration from 653.45 ppt to 5 ppb (hereafter, 10xCFC-12), an increase in N_2O concentration from 316 ppb to 1 ppm (hereafter, $3xN_2O$), an increase tropospheric O_3 concentration used in MacIntosh et al. (2016) by factor of 5 ($5xO_3$), and an increase of present-day black carbon with shorter lifetime by factor of 10 (10xBCSLT). We note that indirect chemical effects are not included in the $3xCH_4$ experiment. Table 1 provides details about the models and the perturbations each one simulated.

The perturbations in GHGs and solar irradiance are relative to the models' baseline simulations, in which the concentration of the GHGs and solar irradiance are either at present-day levels or pre-industrial levels. The perturbations in the aerosols depend on whether it is possible to prescribe aerosol concentrations in the models. For models that are able to prescribe aerosol concentrations, the aerosol perturbations are based on a multi-model mean baseline aerosol concentration in 2000 obtained from the AeroCom Phase II initiative (Myhre et al., 2013). For those that are only able to produce aerosols through emissions, the perturbation is applied by increasing the emissions by the factors listed above. The 10xBCSLT experiment is performed only by models that are able to prescribe aerosol concentrations.

Each perturbation experiment is performed in two configurations: a fixed sea surface temperatures simulation ("fixed SST") and a fully coupled (slab ocean for CAM4 only) simulation. The fixed SST simulations use the SST climatology at either present-day level or pre-industrial level. The fixed SST simulations are at least 15 years and the coupled simulations are at least 100 years.

2.2 Fast response and slow response

When available, SWV mixing ratio is obtained directly from the specific humidity output by each model simulation. For the models that do not output specific humidity (CAM5, GISS-E2-R, and MIROC-SPRINTARS), we calculate specific humidity by multiplying the models' relative humidity by the saturation mixing ratio with respect to ice calculated using model temperature and pressure. Responses of specific humidity and relative humidity in the PDRMIP have been investigated by Hodnebrog et al. (2019), but they focused on water vapor in the troposphere.

We define ΔSWV, the change in SWV mixing ratio in response to a particular perturbation, to be the difference between SWV in the perturbed coupled run and that in the baseline coupled run. As discussed above, the ΔSWV can then be broken down into the two components: the fast response (ΔSWV_{fast}) and slow response (ΔSWV_{slow}). We compute results in the tropical lower stratosphere (70 hPa, 30°N-30°S, hereafter, TLS), in the northern hemispheric (NH) lowermost stratosphere (50°N-90°N at 200 hPa, hereafter, NH LMS), and in the southern hemispheric (SH) lowermost stratosphere (50°S-90°S at 200 hPa, hereafter, SH LMS). Most previous studies have focused on response of water vapor in the TLS (e.g., Gettelman et al., 2010; Shu et al., 2011; Smalley et al., 2017). But recent studies report that the climate is most sensitive to changes in water vapor in the LMS (Solomon et al., 2010; Dessler et al., 2013; Banerjee et al., 2019), so we also investigate that region.

We use the fixed SST simulations to get ΔSWV_{fast}, the rapid adjustment in SWV before sea surface temperature changes. ΔSWV_{fast} is the difference between the SWV mixing ratio averaged over the last 10 years in the fixed SST run with the forcing perturbation and the SWV mixing ratio averaged over the last 10 years in the fixed SST baseline simulation. The fixed SST runs have some warming of the land-surface, meaning that our fast response includes a contribution from warming land-surface. We expect this will have a small impact on our results, but it remains one of the uncertainties in our analysis.

Deleted: change

Deleted: the

Deleted: run with the baseline atmosphere.

We calculate ΔSWV_{slow} as ΔSWV minus ΔSWV_{fast}. To estimate the time series of ΔSWV_{slow}, we use annual mean ΔSWV over the entire coupled run period (at least 100 years) minus the ten-year average ΔSWV_{fast}. To estimate equilibrium ΔSWV_{slow}, we use a regression method similar to the methodology introduced by Gregory et al. (2004). The basic concept is that we regress the annual mean global average net downward radiative flux (R) at the top of atmosphere (TOA) against the annual mean ΔSWV averaged at TLS, NH LMS, or SH LMS. The equilibrium ΔSWV is where the linear fit intercepts at R=0. Then we simply subtract ΔSWV_{fast} from the equilibrium ΔSWV to estimate equilibrium ΔSWV_{slow}.

These regressions can be very noisy and yield highly uncertain parameters, particularly for perturbations with relatively small amounts of radiative forcing and warming. To account for this, we first fit the R and ΔSWV time series using an exponential function ($y(t) = b + a1 \cdot e^{-t/\tau 1} + a2 \cdot e^{-t/\tau 2}$), and then do the regression using the fitted time series. For fully coupled models, we constrain $\tau 1$ to be within the range of 4 ± 2 years and $\tau 2$ to be within the range of 250 ± 70 years; for CAM4, in which the atmosphere is coupled to a slab ocean, we constrain $\tau 1$ to be within the range of 4 ± 2 years. We then compute the best fit of all parameters. The ranges for the time constants are based on previous estimations of climate system time scales (Geoffroy et al., 2013). We estimate the ΔSWV-intercept at R=0 by regressing the fitted R and ΔSWV data over the last 30 years, since the relation between R and ΔSWV is not necessarily linear over the entire 100-year period. The slow and fast responses of other variables, such as global average surface temperatures and cold point temperatures are computed using the same method.

We tested this method in a climate model that nearly reaches the equilibrium climate state. We analysed runs of the fully coupled Max Planck Institute Earth System Model version 1.1 (MPI-ESM1.1) (Maher et al., 2019), which has a transient climate response and an effective climate sensitivity near the middle of the CMIP5 ensemble range (Adams and Dessler, 2019; Dessler, 2020). It includes a 2000-year preindustrial control run and a 2614-year abruptly quadrupled CO_2 run. The values of ΔSWV averaged over the last 30 years of the 4xCO_2 run relative to the control run are 4.60 ppmv in the TLS, 22.40 ppmv in the NH LMS, and 9.69 ppmv in the SH LMS. We expect this to be close to equilibrium ΔSWV because the trend in global average surface temperature over the last 500 years of the 4xCO_2 run is 0.02 K per century. We use the regression method to estimate the equilibrium ΔSWV using MPI-ESM1.1 water vapor mixing ratio time series over the first 100 years and obtain estimates of 4.38 ppmv in the TLS, 20.01 ppmv in the NH LMS, and 9.07 ppmv in the SH LMS; these yield differences of 0.22 ppmv in the TLS, 2.39 ppmv in the NH LMS, and 0.62 ppmv in the SH LMS. Thus, our method underestimates the true equilibrium value by 5% in the TLS, 11% in the NH LMS, and 6% in the SH LMS.

Deleted: (Adams and Dessler, 2019; Dessler, 2020).

Uncertainty for slow and fast responses of different quantities shown in this paper are obtained from Monte Carlo samples as follows: For each perturbation, we randomly sample with replacement 100,000 times for each model that performed that perturbation and from these samples compute the 2.5%-97.5% percentiles.

3. Results

3.1 The slow stratospheric water vapor response

We show equilibrium ΔSWV_{slow} and its percentage contribution to the total equilibrium ΔSWV in Figure 1. We show results in the TLS (Figs. 1a and 1d), in the NH LMS (Figs. 1b and 1e), and the SH LM (Figs. 1c and 1f). In evaluating the absolute magnitude of ΔSWV_{slow} in the first column of Fig. 1, we normalize the equilibrium ΔSWV_{slow} using effective radiative forcing (ERF), so that differences in the magnitude of the forcing do not confound our results.

ERF values used in construction of Fig. 1 are plotted in Fig. 2a; they are calculated as the difference in net radiation at the top of atmosphere (TOA) averaged over the last 10 years between the fixed SST perturbed and baseline simulation. Previous studies have computed the ERF in the PDRMIP using various methods (Richardson et al., 2019; Tang et al., 2019). Our calculation uses the same method as Richardson et al. (2019) "ERF_{sst}" and a direct comparison with Richardson et al. (2019) showing good agreement can be found in the supplement (Table S3). The equilibrium global averaged surface temperature changes (ΔTs), estimated using the regression method described in Section 2.2 and normalized by ERF, are plotted in Fig. 2b. The multi-model mean ΔTs/ERF shows general agreement across different perturbations. This quantity is the inverse of the feedback parameter λ (e.g. Dessler and Zelinka, 2015), so Fig. 2b implies that the climate sensitivity to these different perturbations is similar, which also agrees with Richardson et al. (2019). We list the ERF and ΔTs quantities for each model

Deleted: after the atmospheric perturbation (e.g., the addition of CO_2), but before the surface has warmed. In all cases, we calculate this by differencing the average of the last 10 years of the fixed SST run with the perturbed atmosphere from the same quantity in the fixed SST run with the baseline atmosphere. The equilibrium global averaged surface temperature changes (ΔTs), estimated using the regression method described in Section 2.2 and normalized by ERF, are plotted in Fig. 2b. The ensemble average ΔTs/ERF shows general agreement across different perturbations. This quantity is the inverse of the feedback parameter λ (e.g. Dessler and Zelinka, 2015), so Fig. 2b implies that the climate sensitivity to these different perturbations is similar (Richardson et al., 2019). We also list the and perturbation in Table S1.

In each region, the magnitude of multi-model mean ΔSWV_{slow}/ERF shows general agreement for different perturbations. The magnitudes of ΔSWV_{slow}/ERF in the LMS are larger than those in the TLS (Figs. 1b-c). This is consistent with previous studies, which showed that the long-term trend in SWV over the century in climate models is largest near the LMS tropopause (Dessler et al., 2013; Huang et al., 2016; Banerjee et al., 2019). This reflects different transport pathways into the LMS, including the downward transport by the Brewer-Dobson circulation, quasi-horizontal isentropic mixing from tropical troposphere, and convective influence (Dessler et al., 1995; Holton et al., 1995; Plumb, 2002; Gettelman et al., 2011).

Deleted: ensemble average

Deleted: tend to be

In the LMS, the multi-model mean $\Delta SWV_{slow}/\Delta SWV$ ratio is close to 100% for many perturbations (Figs. 1e-f). The latitude band (50º-90º) we choose is somewhat arbitrary, so in the supplement (Fig. S1), we also show ΔSWV_{slow}/ERF and $\Delta SWV_{slow}/\Delta SWV$ ratio for water vapor averaged at 200 hPa between 30 and 50 degree latitudes in the NH and SH, respectively, which also show that the ΔSWV_{slow} plays a dominant role and contributes to close to 100% of the total ΔSWV for most perturbations. In the TLS, the multi-model mean $\Delta SWV_{slow}/\Delta SWV$ ratio is generally above 50%, with a few exceptions. We will discuss this in detail in Section 3.3.

Deleted: ensemble average

Deleted: ensemble average

We note that inter-model variability in ΔSWV_{slow}/ERF and ΔSWV_{slow} is generally consistent for different perturbations. For example, HadGEM3 produces larger responses than the rest of the models for most perturbations (Figs. 1a-c, Table S1). GISS-E2-R and MIROC-SPRINTARS have ΔSWV_{slow}/ERF and ΔSWV_{slow} values generally below the rest of the models (Figs. 1a-c, Table S1). We have not further investigated the causes of these differences among models; this clearly warrants further investigation.

Deleted: ensemble

Deleted:), likely connected to larger surface warming per ERF than the rest of the ensemble (Fig. 2b

Deleted: ensemble (Figs. 1a-c, Table S1), likely connected to smaller surface temperature changes per ERF (Fig. 2b).

We also note that CAM5, CanESM2, and MIROC-SPRINTARS produce negative TLS ΔSWV_{slow}/ERF for 10xBC. These negative values are partly contributed by artifacts of the method we use to estimate equilibrium ΔSWV_{slow}, which is the residual of the total equilibrium ΔSWV minus ΔSWV_{fast}. When differencing two numbers with similar magnitudes, the residual may be quite uncertain. However, the negative values here do not necessarily mean that a BC-induced surface warming results in negative SWV slow response. The direct regression between ΔSWV_{slow} and surface temperature change described in the next section more accurately describe the relationship for these cases.

3.2 The slow stratospheric water vapor response and the surface temperature change

Our results show that, in most climate perturbations analyzed in this study, the equilibrium response of water vapor in both the TLS and the LMS is dominated by ΔSWV_{slow}, which is the component mediated by sea surface temperature change. To directly quantify how SWV responds to surface temperature across a range of different climate change mechanisms, we linearly regress the time series of annual mean ΔSWV_{slow} over the entire period of the coupled simulations (at least 100 years) against the time series of annual mean global averaged surface temperature change (ΔTs). We do this regression for each model and perturbation separately. This is similar to the analysis of Banerjee et al. (2019), who did this for quadrupled CO_2 perturbation, but we do this for multiple perturbations.

The scatter plot for each perturbation and model is shown in supplement (Figures S3-5). For most perturbations and models, the ΔSWV_{slow} time series in both the TLS and the LMS is positively correlated with the ΔTs time series, supporting the hypothesis that the surface temperature change contributes to the long-term trend in SWV for most cases.

Deleted: S1-3

Figure 3 shows the slopes of the regression for all perturbations and models. The corresponding slope values are listed in Table S4. We also list slopes in the unit of %/K in Table S5. The uncertainty of the slopes is obtained from Monte Carlo samples: For each model and perturbation, we first randomly sample the slope 100,000 times, assuming a Gaussian distribution. Then, for each perturbation, we sample from the slope distributions with replacement 100,000 times for each model that performed that perturbation and from these samples compute the multi-model mean and 2.5%-97.5% percentiles.

Deleted: ensemble average and

Deleted: are

Deleted: ensemble

In both the TLS and LMS, the slopes from different perturbations show general agreement (Fig. 3); this is also true for water vapor averaged at 200 hPa between 30 and 50 degree latitudes in the NH and SH (Fig. S2). In the TLS, the multi-model and multi-perturbation average slope is 0.35 ppmv K^{-1} with a 95% confidence interval of 0.28-0.44 ppmv K^{-1} (Fig. 3a). The LMS ΔSWV_{slow} time series has stronger correlations with the ΔTs time series (Figures S3-5) and produces larger sensitivities (Figs. 3b-c). Specifically, the multi-model and multi-perturbation mean slope is 2.1 ppmv K^{-1} in the NH, and is 0.97 ppmv K^{-1} in the SH, with 95% confidence intervals of 1.82-2.39 ppmv K^{-1} and 0.79-1.15 ppmv K^{-1}, respectively. Our results are similar to those of Dessler et al. (2013) and Smalley et al. (2017) despite the fact that they used 500-hPa temperature as their regressor.

Deleted: 3). In the TLS, the ensemble and

Deleted: S1-3) and produces larger sensitivities (Figs. 3b-c). Specifically, the ensemble and perturbation average slope is 2.1 ppmv K^{-1} in the NH, and is 0.97 ppmv K^{-1} in the SH, with 95% confidence intervals of 1.82-2.39 ppmv K^{-1} and 0.79-1.15 ppmv K^{-1}, respectively. The larger LMS SWV sensitivity reflects a different mix of transport pathways into the LMS compared to the TLS (Dessler et al., 1995; Holton et al., 1995; Plumb, 2002; Gettelman et al., 2011).

We show that the relation between ΔSWV_{slow} and ΔTs time series can be extended to the entire stratosphere (Figs. 4a). We re-gridded the zonal mean ΔSWV_{slow} from all models and perturbations onto the same pressure-latitude grid (10 hPa above 100 hPa and 50 hPa below 100 hPa, 4 degrees latitude) and regress the ΔSWV_{slow} time series at each grid point against global average ΔTs time series. The multi-model and multi-perturbation average slope of the linear fit at each grid point is shown in Fig. 4a (Figures for each individual perturbation are shown in Fig. S6). Since the vertical gradient of water vapor is large, we plot the percentage change of mixing ratio per degree K relative to the baseline. Lapse rate tropopause, the lowest level where the lapse rate decreases to 2 K km^{-1}, also plotted, is obtained using the atmospheric temperatures from the baseline coupled run and multi-model mean.

Deleted: ensemble

Deleted: S4

Deleted: ensemble averaged.

We clearly see the larger sensitivity of ΔSWV_{slow} to ΔTs in the LMS than in the overworld. In the LMS, the slope has a hemispheric asymmetry, with larger values in the NH. This is consistent with previous studies, which showed that isentropic transport brings more tropospheric water vapor to the NH than the SH (Pan et al., 1997, 2000; Dethof et al., 1999, 2000;

Ploeger et al., 2013). In addition, convective moistening may be more important to the NH due to more land in the NH and, consequently, more convection (Dessler and Sherwood, 2004; Smith et al., 2017; Ueyama et al., 2018; Wang et al., 2019). We also large responses in the tropical upper troposphere, which is the main part of the tropospheric water vapor feedback. The sensitivity declines as one ascends through the TTL. Once above the TTL, the sensitivity in the overworld is relatively uniform with altitude.

3.3 The fast stratospheric water vapor response

Figure 1 also shows the ΔSWV_{fast} normalized by the ERF (Figs. 1g-i) as well as its contribution to total equilibrium ΔSWV (Figs. 1j-l). As discussed previously, ΔSWV_{fast} is the rapid adjustment in SWV before the sea surface temperatures respond. For most perturbations, especially in the LMS, ΔSWV_{fast}/ERF is smaller than ΔSWV_{slow}/ERF, with a magnitude of a few tenths of a ppmv·$(Wm^{-2})^{-1}$.

For $2xCO_2$, the near-zero TLS $\Delta SWVf_{ast}$/ERF is the result of cancellation between cooling by a strengthening Brewer-Dobson circulation and increased local radiative heating (Lin et al., 2017). Some other GHG forcing agents, however, produce larger TLS ΔSWV_{fast}/ERF and contributions in the TLS. The multi-model mean ΔSWV_{fast} from 10xCFC-12 and 10xCFC-11 contribute about half of the total ΔSWV, respectively (Fig. 1j). This is a consequence of halocarbons producing more TTL warming per Wm^{-2} by efficiently absorbing upwelling longwave radiation from the troposphere in the atmospheric window (Forster et al., 1997; Jain et al., 2000; Forster and Joshi, 2005). Fig. 5 shows the fast temperature response per unit ERF due to different perturbations and it shows heating in the TTL for both 10xCFC-12 and 10xCFC-11.

The $3xCH_4$ also includes some models that produce large TLS ΔSWV_{fast}/ERF magnitudes. This is likely due to TTL heating (Fig. 5) by CH_4 shortwave absorption, which is explicitly treated in some models, including CAM5, CanESM2, MPI-ESM, and MIROC-SPRINTARS (Smith et al., 2018). These models are also the ones that produce the largest TLS ΔSWV_{fast} contributions (Figs. 1g and 1j).

Increases of tropospheric O_3 (in the $5xO_3$ experiment) reduce the upwelling longwave radiation, which cools the stratosphere (Ramaswamy and Bowen, 1994; Berntsen et al., 1997; Forster et al., 1997). The longwave radiation absorbed heats the TTL region (Fig. 5), resulting in larger TLS ΔSWV_{fast}/ERF magnitude than ΔSWV_{slow}/ERF and larger contributions to total equilibrium ΔSWV (77%) (Figs. 1g and 1j). There is also heating in the LMS, resulting in larger LMS ΔSWV_{fast}/ERF magnitude than ΔSWV_{slow}/ERF (Figs. 1h-j). We note that our conclusion on $5xO_3$ is based on only one model, MIROC-SPRINTARS.

ΔSWV_{fast} from 10xBC dominates total equilibrium ΔSWV in the TLS, with multi-model mean contribution of 84%. The magnitude of the multi-model mean ΔSWV_{fast}/ERF from 10xBC is also larger than any other perturbations in each region.

Deleted: see

Deleted: values

Deleted:

Deleted: change

Deleted: due to the perturbation, but

Deleted: temperature has responded

Deleted: The ensemble average ΔSWV_{fast} from 10xCFC-12 and 10xCFC-11 contribute about half of the total ΔSWV, respectively (Fig. 1j). This is a consequence of halocarbons producing more TTL warming per Wm^{-2} by efficiently absorbing upwelling longwave radiation from the troposphere in the atmospheric window (Jain et al., 2000).

Deleted: Increases of tropospheric O_3 ($5xO_3$) reduce the shortwave radiation absorption by stratospheric O_3, which cools the stratosphere (Fig. 5). Meanwhile, the O_3 in the upper troposphere absorbs short wave radiation and heats the TTL (Fig. 5), which results

Moved down [1]: in larger TLS ΔSWV_{fast}/ERF magnitude than ΔSWV_{slow}/ERF and larger contributions to total equilibrium ΔSWV (77%) (Figs. 1g and 1j).

Deleted: Tropospheric O_3 is also transported to the LMS region, which heats the LMS by absorbing short wave radiation and results in larger LMS ΔSWV_{fast}/ERF magnitude than ΔSWV_{slow}/ERF (Figs.

Moved down [2]: 1h-j). We note that our conclusion on $5xO_3$ is based on only one model, MIROC-SPRINTARS.¶

Deleted: multiple

Deleted: larger

Deleted: and contributions than ΔSWV_{slow}/ERF. Figure 5 shows

Deleted: for $3xCH_4$. The TTL heating could be due to the shortwave absorption

Deleted: larger than 50% in $3xCH_4$

Moved (insertion) [1]

Deleted: ΔSWV_{fast} from 10xBC dominates total equilibrium ΔSWV in the TLS, with ensemble average contribution of 84%. The magnitude of the ensemble average

Moved (insertion) [2]

Deleted: ΔSWV_{fast}/ERF from 10xBC is also larger than any other perturbations in each region. This occurs because the 10xBC strongly absorbs shortwave radiation, causing large heating of the tropopause region in both the tropics and extra-tropics. Figure 5 shows the 10xBC gives by far the most warming per unit ERF.¶

This occurs because the 10xBC strongly absorbs shortwave radiation, causing large heating of the tropopause region in both the tropics and extra-tropics. Figure 5 shows the 10xBC gives by far the most warming per unit ERF, which is consistent with the vertical profile of fast temperature response shown in Stjern et al. (2017).

The 10xBC ΔSWV_{fast}/ERF in the NH and SH LMS contributes to about 50% of the total equilibrium ΔSWV, with smaller magnitudes in the SH (Figs. 1h-i and 1k-l). This is because the total amount of black carbon is smaller in the SH (Myhre et al., 2017), since black carbon is a combustion product and is predominantly emitted over the NH continents (Ramanathan and Carmichael, 2008). The 10xBCSLT ΔSWV_{fast} also contributes about 50% of the total 10xBCSLT ΔSWV. The 10xBCSLT does not produce as strong a ΔSWV_{fast}/ERF as 10xBC, since the reduction in BC lifetime leads to less BC in the TTL and therefore less heating per unit ERF.

We quantify control of TLS ΔSWV_{fast} by the fast TTL temperature adjustments across a range of different climate perturbations by regressing the TLS ΔSWV_{fast} against the fast response of the cold point temperature (ΔTCP_{fast}). To estimate ΔTCP_{fast} in the models, we first find the minimum temperature in the profile at each grid point in the fixed SST runs (no interpolation is done, we simply find the minimum temperature on the output model levels). These minimum temperatures are then averaged between 30°N – 30°S to yield TCP_{fast} in each run. ΔTCP_{fast} is the difference between TCP_{fast} in the perturbed model run minus that in the baseline runs.

We find that TLS ΔSWV_{fast} is strongly correlated with ΔTCP_{fast} across all perturbations and models (Fig. 6a), with a slope of 0.52 ppmv K^{-1} and a 95% confidence interval of 0.43 to 0.61 ppmv K^{-1}. Randel and Park (2019) pointed out that the slope from the Clausius-Clapeyron relationship evaluated near the tropical tropopause is close to this value, about 0.5 ppmv K^{-1}. We also tested the relationship between TLS ΔSWV_{slow} and slow response of the cold point temperature (ΔTCP_{slow}) across all perturbations and models, yielding a slope of 0.72 ppmv K^{-1}. However, for the slow response, correlation does not necessarily prove causality, since Dessler et al. (2016) showed that, in two climate models at least, a significant fraction of the long-term trend was due to increases in convective moistening, which bypasses the TTL cool trap. Therefore this relationship for the slow response could arise from either TCP control or a process that correlates with it, such as deep convective injection of ice, or some combination.

We also separately plot the slopes between ΔSWV_{fast} and ΔTCP_{fast} for each perturbation (Figs. 6d-f). For the perturbations that have more than five participating models, including $2xCO_2$, $3xCH_4$, 2%Solar, 10xBC, $5xSO_4$, and 10xCFC-12, we calculate the linear regression between ΔSWV_{fast} and ΔTCP_{fast} from the models and show the slopes and 95% confidence intervals. For the perturbations that have fewer participating models, including 10xCFC11, $3xN_2O$, $5xO_3$, and 10xBCSLT, we plot the ratio $\Delta SWV_{fast}/\Delta TCP_{fast}$ and show only the multi-model mean. The slopes produced by different perturbations show general agreement (Fig. 6d). The larger uncertainty in the slopes produced by 2%Solar and 10xCFC-12 occurs because both the ΔTCP_{fast} and ΔSWV_{fast} produced by different models are similar and therefore the slope of the linear regression is

Deleted: ensemble averages.

uncertain. Overall, we find that the fast response of TTL temperature is a good predictor for the TLS ΔSWV_{fast} across a range of different climate mechanisms and across multiple models.

For the LMS ΔSWV_{fast}, the ΔTCP_{fast} does not show a control as strong as that in the TLS (Figs. 6b-c) due to the fact that TTL temperatures are only one factor that influences the LMS. In addition, the regression between ΔSWV_{fast} and ΔTCP_{fast} across all perturbations at each grid point in the pressure-latitude domain shows that the slope (% K^{-1}) follows the transport pattern of the BDC (Fig. 4b). The slope is large in the tropical overworld stratosphere and become weaker as one moves poleward and downward in the extra-tropics below 150 hPa. The value is lower in the LMS, again consistent with the fact that water vapor in the LMS is controlled by several processes, not just TTL cold-point temperature. Clearly, more work on this is warranted.

4. Historical changes in SWV

Deleted: Summary¶

Given the importance of SWV change, we now ask whether our results can help us understand historical variations in TLS ΔSWV over 1980-2010 (Figure 7). To do this, we estimate historical values of ΔSWV_{slow} and ΔSWV_{fast} based on the PDRMIP results, historical surface temperature change, and historical radiative forcing. For the slow component (blue in Fig. 7a), we multiply 0.35 ppmv K^{-1}, the multi-model multi-perturbation mean sensitivity of the PDRMIP TLS ΔSWV_{slow} to ΔT_s, by the historical surface temperature change over 1980-2010. For the fast component (orange in Fig. 7a), we multiply the multi-model mean PDRMIP TLS ΔSWV_{fast}/ERF value for each perturbation by the corresponding historical radiative forcing and then sum it up. We also show the fast component of the historical ΔSWV contributed by each historical forcing agent in Fig. 7b. This is similar to the analysis done by Hodnebrog et al. (2019) in their Figure 6, where they used this method to estimate the historical water vapor lifetime change based on the PDRMIP results.

The historical surface temperature change and radiative forcing data used in this analysis are listed in Table 2. The historical radiative forcing we use here is defined as the change in net downward radiative flux at the tropopause, after adjustments in the stratospheric temperatures, while the surface and troposphere are held unperturbed (Myhre et al. 2013). This is different from the ERF we use in the PDRMIP calculations, which introduced uncertainties in the fast component of the historical ΔSWV we estimate based on PDRMIP.

Figure 7a shows our estimate that climate change over 1980-2010 has increased TLS SWV by 0.51±0.16 ppmv (Fig. 7a). 36% is due to the slow component, although this is probably an overestimate because our sensitivity value estimated using the PDRMIP results are for long-term. We find the rest of the ΔSWV, 64%, is due to the fast component, mainly from black carbon. We have also calculated the SWV sensitivity and SWV fast response over 35°N-45°N between 100-80 hPa to re-compute the historical 1980-2010 ΔSWV using the same method, which is 0.65±0.20 ppmv. This value shows reasonable agreement with the SWV increase measured by Hurst et al. (2011) of 0.71±0.26 ppmv over Boulder between 16-18 km over

1980-2010.

Dessler et al. (2014) and Hegglin et al. (2014) argue that there is not a detectible trend over this period. Such a conclusion is not inconsistent with ours because any actual trend estimate has to contend with short-term interannual variability (i.e, like that from the QBO and Brewer-Dobson Circulation variability), which can mask a small trend. Our estimate of the trend is based on sensitivity estimated from 100 year-run and therefore short-term interannual variability has a small impact. Given continuous reliable long-term SWV observation record in the future, one will be able to better test the model-predicted values.

For the fast component of the estimated historical ΔSWV, radiative forcing by BC plays the dominant role (Fig. 7b). Uncertainties exist in the historical BC radiative forcing we use in this analysis, which is shown in the IPCC AR5 (Myhre et al. 2013). In addition, Allen et al. (2019) pointed out that the radiative effect by BC in the PDRMIP is different from that shown in models using observationally constrained aerosol forcing, which may overestimate the heating in the UTLS region. However, Allen et al. (2019) also noted that uncertainties exist in their observationally constrained aerosol forcing. The uncertainties in the impact of BC forcing on SWV clearly merit more analysis in the future.

5. Conclusions

It is of great interest for the climate community to understand how SWV changes when the climate changes since SWV plays an important role in the Earth's radiative budget and stratospheric ozone chemistry (Solomon et al., 1986, 2010; Dvortsov and Solomon, 2001; Forster and Shine, 2002). In this study, we investigate the response of stratospheric water vapor (SWV) to a range of different climate forcing mechanisms using a multi-model and multiple forcing agent framework. We use output from nine CMIP5 models participating the PDRMIP. Each model performs a baseline and up to 10 climate perturbation experiments, including 2xCO_2, 3xCH_4, 2%Solar, 10xBC, 5xSO_4, 10xCFC-11, 10xCFC-12, 3xN_2O, 5xO_3, and 10xBCSLT (Table 1). Each perturbation is performed in two configurations, including fixed SST simulations (at least 15 years) and fully coupled simulations (at least 100 years).

To better understand the SWV response (ΔSWV), we partition it into two parts: the slow response (ΔSWV_{slow}) and the fast response (ΔSWV_{fast}). The ΔSWV_{fast} is the change in response to a perturbation on short time scales, before the surface temperature has responded. ΔSWV_{slow} occurs on longer time scales and is coupled to the surface temperature change. Our results show that, for most perturbations, ΔSWV in the tropical lower stratosphere (TLS) and in the lowermost stratosphere (LMS) (200 hPa, 50°N-90°N and 50°S-90°S) is dominated by ΔSWV_{slow} (Fig. 1).

Analysis of ΔSWV_{slow} shows that a warming surface increases SWV (Figures S3-5). Furthermore, the response of SWV to the surface temperature change has a similar sensitivity across different climate perturbations in both the overworld

Deleted: S1-3

stratosphere and the lowermost stratosphere (Figs. 3 and 4a). Specifically, the multi-model and multi-perturbation mean slope is 0.35 ppmv K^{-1} in the TLS, 2.1 ppmv K^{-1} in the northern hemispheric (NH) LMS, and 0.97 ppmv K^{-1} in the southern hemispheric (SH) LMS (Fig. 3).

Deleted: ensemble

Deleted: average

ΔSWV_{slow} in the LMS is more sensitive to ΔTs than the tropical overworld, reflecting different transport pathways into the LMS compared to the overworld (Dessler et al., 1995; Holton et al., 1995; Plumb, 2002; Gettelman et al., 2011). The ΔSWV_{slow} in the NH LMS is more sensitive than the SH LMS, consistent with hemispheric asymmetries in the isentropic transport and convective moistening reported by previous studies (Pan et al., 1997, 2000; Dethof et al., 1999, 2000; Dessler and Sherwood, 2004; Ploeger et al., 2013; Smith et al., 2017; Ueyama et al., 2018; Wang et al., 2019).

Deleted: even

The fast response of SWV from most perturbations are weak compared to the slow response and therefore plays a smaller role in ΔSWV (Fig. 1). In the TLS, for forcing agents that directly heat tropopause levels (Fig. 5), ΔSWV_{fast} makes a larger contribution to ΔSWV. In particular, when climate is perturbed by 10xBC, the ΔSWV_{fast} dominates the ΔSWV_{slow} and has larger magnitude than any other perturbed simulations. This occurs because black carbon absorbs shortwave radiation in the atmosphere and directly heats the temperatures at tropopause levels. Other forcing agents also heat the tropopause levels and increase ΔSWV_{fast} through absorption of shortwave radiation or longwave radiation at the atmospheric window range ($3xCH_4$, $5xO_3$, 10xBCSLT, 10xCFC-12, 10xCFC-11), but are not as strong as 10xBC.

Deleted: However

Deleted: in both the TLS and LMS.

The TLS ΔSWV_{fast} is controlled by the fast response of the cold point temperature across different climate change mechanisms (Fig. 6), with a slope of 0.52 ppmv K^{-1}, which is consistent with the Clausius-Clapeyron relationship evaluated near the tropical tropopause (Randel and Park, 2019). The control of cold point temperature fast response over ΔSWV_{fast} is stronger in the tropical overworld and becomes weaker at higher latitudes and altitudes below 150 hPa in the LMS (Fig. 4b).

Deleted: in the LMS

Data availability: The PDRMIP data can be downloaded from this website: https://cicero.oslo.no/en/PDRMIP.

Competing interests. The authors declare that they have no conflict of interest.

Author contribution: Xun Wang performed analyses and wrote the paper. Andrew E. Dessler provided the conceptualization, guidance, and editing.

Deleted: original draft.

Acknowledgments: This work was supported by NASA grants 80NSSC18K0134 and 80NSSC19K0757. This work was also supported by the National Center for Atmospheric Research, which is a major facility sponsored by the National Science Foundation under Cooperative Agreement No. 1852977. Any opinions, findings and conclusions or recommendations expressed in this material do not necessarily reflect the views of the National Science Foundation. We would like to acknowledge the PDRMIP modelling groups and helpful discussions with Andrew Gettelman and William Randel.

Deleted: . We acknowledge

References.

Adams, B. K. and Dessler, A. E.: Estimating Transient Climate Response in a Large-Ensemble Global Climate Model Simulation, Geophys. Res. Lett., 46(1), 311–317, doi:10.1029/2018GL080714, 2019.

Allen, R. J., Amiri-Farahani, A., Lamarque, J.-F., Smith, C., Shindell, D., Hassan, T. and Chung, C. E.: Observationally constrained aerosol–cloud semi-direct effects, npj Clim. Atmos. Sci., 2(1), 16, doi:10.1038/s41612-019-0073-9, 2019.

Arora, V. K., Scinocca, J. F., Boer, G. J., Christian, J. R., Denman, K. L., Flato, G. M., Kharin, V. V., Lee, W. G. and Merryfield, W. J.: Carbon emission limits required to satisfy future representative concentration pathways of greenhouse gases, Geophys. Res. Lett., 38(5), n/a-n/a, doi:10.1029/2010GL046270, 2011.

Banerjee, A., Chiodo, G., Previdi, M., Ponater, M., Conley, A. J. and Polvani, L. M.: Stratospheric water vapor: an important climate feedback, Clim. Dyn., doi:10.1007/s00382-019-04721-4, 2019.

Bellouin, N., Rae, J., Jones, A., Johnson, C., Haywood, J. and Boucher, O.: Aerosol forcing in the Climate Model Intercomparison Project (CMIP5) simulations by HadGEM2-ES and the role of ammonium nitrate, J. Geophys. Res., 116(D20), D20206, doi:10.1029/2011JD016074, 2011.

Berntsen, T. K., Isaksen, I. S. A., Myhre, G., Fuglestvedt, J. S., Stordal, F., Larsen, T. A., Freckleton, R. S. and Shine, K. P.: Effects of anthropogenic emissions on tropospheric ozone and its radiative forcing, J. Geophys. Res. Atmos., 102(D23), 28101–28126, doi:10.1029/97JD02226, 1997.

Brasseur, G. P. and Solomon, S.: Aeronomy of the Middle Atmosphere, Springer Netherlands, Dordrecht., 2005.

Collins, W. J., Bellouin, N., Doutriaux-Boucher, M., Gedney, N., Halloran, P., Hinton, T., Hughes, J., Jones, C. D., Joshi, M., Liddicoat, S., Martin, G., O'Connor, F., Rae, J., Senior, C., Sitch, S., Totterdell, I., Wiltshire, A. and Woodward, S.: Development and evaluation of an Earth-System model – HadGEM2, Geosci. Model Dev., 4(4), 1051–1075, doi:10.5194/gmd-4-1051-2011, 2011.

Dessler, A. E.: Potential Problems Measuring Climate Sensitivity from the Historical Record, J. Clim., 33(6), 2237–2248, doi:10.1175/JCLI-D-19-0476.1, 2020.

Dessler, A. E. and Sherwood, S. C.: Effect of convection on the summertime extratropical lower stratosphere, J. Geophys. Res. Atmos., 109(D23), doi:10.1029/2004JD005209, 2004.

Dessler, A. E. and Zelinka, M. D.: Climate Feedbacks, in Encyclopedia of Atmospheric Sciences, edited by P. J. North G. R. and F. Zhang, Academic Press, Oxford, 2015.

Dessler, A. E., Hintsa, E. J., Weinstock, E. M., Anderson, J. G. and Chan, K. R.: Mechanisms controlling water vapor in the lower stratosphere: “A tale of two stratospheres,” J. Geophys. Res., 100(D11), 23167, doi:10.1029/95JD02455, 1995.

Dessler, A. E., Schoeberl, M. R., Wang, T., Davis, S. M. and Rosenlof, K. H.: Stratospheric water vapor feedback, Proc. Natl. Acad. Sci., 110(45), 18087–18091, doi:10.1073/pnas.1310344110, 2013.

Dessler, A. E., Schoeberl, M. R., Wang, T., Davis, S. M., Rosenlof, K. H. and Vernier, J.-P.: Variations of stratospheric water vapor over the past three decades, J. Geophys. Res. Atmos., 119(22), 12,588-12,598, doi:10.1002/2014JD021712, 2014.

Dessler, A. E., Ye, H., Wang, T., Schoeberl, M. R., Oman, L. D., Douglass, A. R., Butler, A. H., Rosenlof, K. H., Davis, S. M. and Portmann, R. W.: Transport of ice into the stratosphere and the humidification of the stratosphere over the 21st century, Geophys. Res. Lett., 43(5), 2323–2329, doi:10.1002/2016GL067991, 2016.

Dethof, A., O’Neill, A., Slingo, J. M. and Smit, H. G. J.: A mechanism for moistening the lower stratosphere involving the Asian summer monsoon, Q. J. R. Meteorol. Soc., 125(556), 1079–1106, doi:10.1002/qj.1999.49712555602, 1999.

Dethof, A., O’Neill, A. and Slingo, J.: Quantification of the isentropic mass transport across the dynamical tropopause, J. Geophys. Res. Atmos., 105(D10), 12279–12293, doi:10.1029/2000JD900127, 2000.

Dlugokencky, E.J., J.W. Mund, A.M. Crotwell, M.J. Crotwell, and K.W. Thoning (2020), Atmospheric Carbon Dioxide Dry Air Mole Fractions from the NOAA GML Carbon Cycle Cooperative Global Air Sampling Network, 1968-2019, Version: 2020-07, https://doi.org/10.15138/wkgj-f215

Dlugokencky, E.J., A.M. Crotwell, J.W. Mund, M.J. Crotwell, and K.W. Thoning (2020), Atmospheric Methane Dry Air

Mole Fractions from the NOAA GML Carbon Cycle Cooperative Global Air Sampling Network, 1983-2019, Version: 2020-07, https://doi.org/10.15138/VNCZ-M766

Dlugokencky, E.J., A.M. Crotwell, J.W. Mund, M.J. Crotwell, and K.W. Thoning (2020), Atmospheric Nitrous Oxide Dry Air Mole Fractions from the NOAA GML Carbon Cycle Cooperative Global Air Sampling Network, 1997-2019, Version: 2020-07, https://doi.org/10.15138/53g1-x417

Dufresne, J.-L., Foujols, M.-A., Denvil, S., Caubel, A., Marti, O., Aumont, O., Balkanski, Y., Bekki, S., Bellenger, H., Benshila, R., Bony, S., Bopp, L., Braconnot, P., Brockmann, P., Cadule, P., Cheruy, F., Codron, F., Cozic, A., Cugnet, D., de Noblet, N., Duvel, J.-P., Ethé, C., Fairhead, L., Fichefet, T., Flavoni, S., Friedlingstein, P., Grandpeix, J.-Y., Guez, L., Guilyardi, E., Hauglustaine, D., Hourdin, F., Idelkadi, A., Ghattas, J., Joussaume, S., Kageyama, M., Krinner, G., Labetoulle, S., Lahellec, A., Lefebvre, M.-P., Lefevre, F., Levy, C., Li, Z. X., Lloyd, J., Lott, F., Madec, G., Mancip, M., Marchand, M., Masson, S., Meurdesoif, Y., Mignot, J., Musat, I., Parouty, S., Polcher, J., Rio, C., Schulz, M., Swingedouw, D., Szopa, S., Talandier, C., Terray, P., Viovy, N. and Vuichard, N.: Climate change projections using the IPSL-CM5 Earth System Model: from CMIP3 to CMIP5, Clim. Dyn., 40(9–10), 2123–2165, doi:10.1007/s00382-012-1636-1, 2013.

Dvortsov, V. L. and Solomon, S.: Response of the stratospheric temperatures and ozone to past and future increases in stratospheric humidity, J. Geophys. Res. Atmos., 106(D7), 7505–7514, doi:10.1029/2000JD900637, 2001.

Forster, P. M. D. F. and Joshi, M.: The Role Of Halocarbons In The Climate Change Of The Troposphere And Stratosphere, Clim. Change, 71(1–2), 249–266, doi:10.1007/s10584-005-5955-7, 2005.

Forster, P. M. de F. and Shine, K. P.: Assessing the climate impact of trends in stratospheric water vapor, Geophys. Res. Lett., 29(6), 10-1-10–4, doi:10.1029/2001GL013909, 2002.

Forster, P. M. F., Freckleton, R. S. and Shine, K. P.: On aspects of the concept of radiative forcing, Clim. Dyn., 13(7–8), 547–560, doi:10.1007/s003820050182, 1997.

Fueglistaler, S., Dessler, A. E., Dunkerton, T. J., Folkins, I., Fu, Q. and Mote, P. W.: Tropical tropopause layer, Rev. Geophys., 47, 1–31, doi:10.1029/2008RG000267, 2009.

Gent, P. R., Danabasoglu, G., Donner, L. J., Holland, M. M., Hunke, E. C., Jayne, S. R., Lawrence, D. M., Neale, R. B., Rasch, P. J., Vertenstein, M., Worley, P. H., Yang, Z.-L. and Zhang, M.: The Community Climate System Model Version 4, J. Clim., 24(19), 4973–4991, doi:10.1175/2011JCLI4083.1, 2011.

Geoffroy, O., Saint-Martin, D., Olivié, D. J. L., Voldoire, A., Bellon, G. and Tytéca, S.: Transient Climate Response in a Two-Layer Energy-Balance Model. Part I: Analytical Solution and Parameter Calibration Using CMIP5 AOGCM Experiments, J. Clim., 26(6), 1841–1857, doi:10.1175/JCLI-D-12-00195.1, 2013.

Gettelman, A., Hegglin, M. I., Son, S.-W., Kim, J., Fujiwara, M., Birner, T., Kremser, S., Rex, M., Añel, J. A., Akiyoshi, H., Austin, J., Bekki, S., Braesike, P., Brühl, C., Butchart, N., Chipperfield, M., Dameris, M., Dhomse, S., Garny, H., Hardiman, S. C., Jöckel, P., Kinnison, D. E., Lamarque, J. F., Mancini, E., Marchand, M., Michou, M., Morgenstern, O., Pawson, S., Pitari, G., Plummer, D., Pyle, J. A., Rozanov, E., Scinocca, J., Shepherd, T. G., Shibata, K., Smale, D., Teyssèdre, H. and Tian, W.: Multimodel assessment of the upper troposphere and lower stratosphere: Tropics and global trends, J. Geophys. Res., 115, D00M08, doi:10.1029/2009JD013638, 2010.

Gettelman, A., Hoor, P., Pan, L. L., Randel, W. J., Hegglin, M. I. and Birner, T.: THE EXTRATROPICAL UPPER TROPOSPHERE AND LOWER STRATOSPHERE, Rev. Geophys., 49(3), RG3003, doi:10.1029/2011RG000355, 2011.

Giorgetta, M. A., Jungclaus, J., Reick, C. H., Legutke, S., Bader, J., Böttinger, M., Brovkin, V., Crueger, T., Esch, M., Fieg, K., Glushak, K., Gayler, V., Haak, H., Hollweg, H.-D., Ilyina, T., Kinne, S., Kornblueh, L., Matei, D., Mauritsen, T., Mikolajewicz, U., Mueller, W., Notz, D., Pithan, F., Raddatz, T., Rast, S., Redler, R., Roeckner, E., Schmidt, H., Schnur, R., Segschneider, J., Six, K. D., Stockhause, M., Timmreck, C., Wegner, J., Widmann, H., Wieners, K.-H., Claussen, M., Marotzke, J. and Stevens, B.: Climate and carbon cycle changes from 1850 to 2100 in MPI-ESM simulations for the Coupled Model Intercomparison Project phase 5, J. Adv. Model. Earth Syst., 5(3), 572–597, doi:10.1002/jame.20038, 2013.

Gregory, J. M.: A new method for diagnosing radiative forcing and climate sensitivity, Geophys. Res. Lett., 31(3), L03205, doi:10.1029/2003GL018747, 2004.

Hegglin, M. I., Plummer, D. A., Shepherd, T. G., Scinocca, J. F., Anderson, J., Froidevaux, L., Funke, B., Hurst, D., Rozanov, A., Urban, J., von Clarmann, T., Walker, K. A., Wang, H. J., Tegtmeier, S. and Weigel, K.: Vertical structure of stratospheric water vapour trends derived from merged satellite data, Nat. Geosci., 7(10), 768–776, doi:10.1038/ngeo2236, 2014.

Hodnebrog, Ø., Myhre, G., Samset, B. H., Alterskjær, K., Andrews, T., Boucher, O., Faluvegi, G., Fläschner, D., Forster, P. M., Kasoar, M., Kirkevåg, A., Lamarque, J.-F., Olivié, D., Richardson, T. B., Shawki, D., Shindell, D., Shine, K. P., Stier, P., Takemura, T., Voulgarakis, A. and Watson-Parris, D.: Water vapour adjustments and responses differ between climate drivers, Atmos. Chem. Phys., 19(20), 12887–12899, doi:10.5194/acp-19-12887-2019, 2019.

Holton, J. R., Haynes, P. H., McIntyre, M. E., Douglass, A. R., Rood, R. B. and Pfister, L.: Stratosphere-troposphere exchange, Rev. Geophys., 33(4), 403, doi:10.1029/95RG02097, 1995.

Hoskins, B. J.: Towards a PV-θ view of the general circulation, Tellus A Dyn. Meteorol. Oceanogr., 43(4), 27–36, doi:10.3402/tellusa.v43i4.11936, 1991.

Huang, Y., Zhang, M., Xia, Y., Hu, Y. and Son, S.-W.: Is there a stratospheric radiative feedback in global warming simulations?, Clim. Dyn., 46(1–2), 177–186, doi:10.1007/s00382-015-2577-2, 2016.

Hurrell, J. W., Holland, M. M., Gent, P. R., Ghan, S., Kay, J. E., Kushner, P. J., Lamarque, J.-F., Large, W. G., Lawrence, D., Lindsay, K., Lipscomb, W. H., Long, M. C., Mahowald, N., Marsh, D. R., Neale, R. B., Rasch, P., Vavrus, S., Vertenstein, M., Bader, D., Collins, W. D., Hack, J. J., Kiehl, J. and Marshall, S.: The Community Earth System Model: A Framework for Collaborative Research, Bull. Am. Meteorol. Soc., 94(9), 1339–1360, doi:10.1175/BAMS-D-12-00121.1, 2013.

Hurst, D. F., Oltmans, S. J., Vömel, H., Rosenlof, K. H., Davis, S. M., Ray, E. A., Hall, E. G. and Jordan, A. F.: Stratospheric water vapor trends over Boulder, Colorado: Analysis of the 30 year Boulder record, J. Geophys. Res., 116(D2), D02306, doi:10.1029/2010JD015065, 2011.

Intergovernmental Panel on Climate Change., Houghton, J. T., Intergovernmental Panel on Climate Change., & World Meteorological Organization. (1990). IPCC first assessment report. Geneva: WMO.

Jain, A. K., Briegleb, B. P., Minschwaner, K. and Wuebbles, D. J.: Radiative forcings and global warming potentials of 39 greenhouse gases, J. Geophys. Res. Atmos., 105(D16), 20773–20790, doi:10.1029/2000JD900241, 2000.

Kay, J. E., Deser, C., Phillips, A., Mai, A., Hannay, C., Strand, G., Arblaster, J. M., Bates, S. C., Danabasoglu, G., Edwards, J., Holland, M., Kushner, P., Lamarque, J.-F., Lawrence, D., Lindsay, K., Middleton, A., Munoz, E., Neale, R., Oleson, K., Polvani, L. and Vertenstein, M.: The Community Earth System Model (CESM) Large Ensemble Project: A Community Resource for Studying Climate Change in the Presence of Internal Climate Variability, Bull. Am. Meteorol. Soc., 96(8), 1333–1349, doi:10.1175/BAMS-D-13-00255.1, 2015.

Lin, P., Paynter, D., Ming, Y. and Ramaswamy, V.: Changes of the Tropical Tropopause Layer under Global Warming, J. Clim., 30(4), 1245–1258, doi:10.1175/JCLI-D-16-0457.1, 2017.

MacIntosh, C. R., Allan, R. P., Baker, L. H., Bellouin, N., Collins, W., Mousavi, Z. and Shine, K. P.: Contrasting fast precipitation responses to tropospheric and stratospheric ozone forcing, Geophys. Res. Lett., 43(3), 1263–1271, doi:10.1002/2015GL067231, 2016.

Maher, N., Milinski, S., Suarez-Gutierrez, L., Botzet, M., Dobrynin, M., Kornblueh, L., Kröger, J., Takano, Y., Ghosh, R., Hedemann, C., Li, C., Li, H., Manzini, E., Notz, D., Putrasahan, D., Boysen, L., Claussen, M., Ilyina, T., Olonscheck, D., Raddatz, T., Stevens, B. and Marotzke, J.: The Max Planck Institute Grand Ensemble: Enabling the Exploration of Climate System Variability, J. Adv. Model. Earth Syst., 11(7), 2050–2069, doi:10.1029/2019MS001639, 2019.

Martin, T. H. D. T. G. M., Bellouin, N., Collins, W. J., Culverwell, I. D., Halloran, P. R., Hardiman, S. C., Hinton, T. J., Jones, C. D., McDonald, R. E., McLaren, A. J., O'Connor, F. M., Roberts, M. J., Rodriguez, J. M., Woodward, S., Best, M. J., Brooks, M. E., Brown, A. R., Butchart, N., Dearden, C., Derbyshire, S. H., Dharssi, I., Doutriaux-Boucher, M., Edwards, J. M., Falloon, P. D., Gedney, N., Gray, L. J., Hewitt, H. T., Hobson, M., Huddleston, M. R., Hughes, J., Ineson, S., Ingram, W. J., James, P. M., Johns, T. C., Johnson, C. E., Jones, A., Jones, C. P., Joshi, M. M., Keen, A. B., Liddicoat, S., Lock, A. P., Maidens, A. V, Manners, J. C., Milton, S. F., Rae, J. G. L., Ridley, J. K., Sellar, A., Senior, C. A., Totterdell, I. J., Verhoef, A., Vidale, P. L. and Wiltshire, A.: The HadGEM2 family of Met Office Unified Model climate configurations, Geosci. Model Dev., 4(3), 723–757, doi:10.5194/gmd-4-723-2011, 2011.

Mote, P. W., Rosenlof, K. H., McIntyre, M. E., Carr, E. S., Gille, J. C., Holton, J. R., Kinnersley, J. S., Pumphrey, H. C., Russell III, J. M. and Waters, J. W.: An atmospheric tape recorder: The imprint of tropical tropopause temperatures on stratospheric water vapor, J. Geophys. Res., 101(D2), 3989–4006, doi:10.1029/95JD03422, 1996.

Myhre, G., Highwood, E. J., Shine, K. P. and Stordal, F.: New estimates of radiative forcing due to well mixed greenhouse

gases, Geophys. Res. Lett., 25(14), 2715–2718, doi:10.1029/98GL01908, 1998.
Myhre, G., Samset, B. H., Schulz, M., Balkanski, Y., Bauer, S., Berntsen, T. K., Bian, H., Bellouin, N., Chin, M., Diehl, T., Easter, R. C., Feichter, J., Ghan, S. J., Hauglustaine, D., Iversen, T., Kinne, S., Kirkevåg, A., Lamarque, J.-F., Lin, G., Liu, X., Lund, M. T., Luo, G., Ma, X., van Noije, T., Penner, J. E., Rasch, P. J., Ruiz, A., Seland, Ø., Skeie, R. B., Stier, P., Takemura, T., Tsigaridis, K., Wang, P., Wang, Z., Xu, L., Yu, H., Yu, F., Yoon, J.-H., Zhang, K., Zhang, H. and Zhou, C.: Radiative forcing of the direct aerosol effect from AeroCom Phase II simulations, Atmos. Chem. Phys., 13(4), 1853–1877, doi:10.5194/acp-13-1853-2013, 2013.
Myhre, G., D. Shindell, F.-M. Bréon, W. Collins, J. Fuglestvedt, J. Huang, D. Koch, J.-F. Lamarque, D. Lee, B. Mendoza, T. Nakajima, A. Robock, G. Stephens, T. Takemura and H. Zhang, 2013: Anthropogenic and Natural Radiative Forc- ing. In: Climate Change 2013: The Physical Science Basis. Contribution of Working Group I to the Fifth Assessment Report of the Intergovernmental Panel on Climate Change [Stocker, T.F., D. Qin, G.-K. Plattner, M. Tignor, S.K. Allen, J. Boschung, A. Nauels, Y. Xia, V. Bex and P.M. Midgley (eds.)]. Cambridge University Press, Cambridge, United Kingdom and New York, NY, USA.
Myhre, G., Forster, P. M., Samset, B. H., Hodnebrog, Ø., Sillmann, J., Aalbergsjø, S. G., Andrews, T., Boucher, O., Faluvegi, G., Fläschner, D., Iversen, T., Kasoar, M., Kharin, V., Kirkevåg, A., Lamarque, J.-F., Olivié, D., Richardson, T. B., Shindell, D., Shine, K. P., Stjern, C. W., Takemura, T., Voulgarakis, A. and Zwiers, F.: PDRMIP: A Precipitation Driver and Response Model Intercomparison Project—Protocol and Preliminary Results, Bull. Am. Meteorol. Soc., 98(6), 1185–1198, doi:10.1175/BAMS-D-16-0019.1, 2017.
Neale, R. B., Richter, J. H., Conley, A. J., Park, S., Lauritzen, P. H., Gettelman, A., Williamson, D. L., Rasch, P. J., Vavrus, S. J., Taylor, M. A., Collins, W. D., Zhang, M., and Lin, S.:Description of the NCAR Community Atmosphere Model (CAM 4.0), NCAR Technical Note, NCAR/TN-485+STR, Climate And Global Dynamics Division National Center For Atmospheric Research Boulder, Colorado, USA, 224 pp., 2010. Available at http://www.cesm.ucar.edu/models/ccsm4.0/cam/docs/description/cam4_desc.pdf
http://www.cesm.ucar.edu/models/ccsm4.0/cam/docs/description/cam4_desc.pdf
Otto-Bliesner, B. L., Brady, E. C., Fasullo, J., Jahn, A., Landrum, L., Stevenson, S., Rosenbloom, N., Mai, A. and Strand, G.: Climate Variability and Change since 850 CE: An Ensemble Approach with the Community Earth System Model, Bull. Am. Meteorol. Soc., 97(5), 735–754, doi:10.1175/BAMS-D-14-00233.1, 2016.
Pan, L., Solomon, S., Randel, W., Lamarque, J.-F., Hess, P., Gille, J., Chiou, E.-W. and McCormick, M. P.: Hemispheric asymmetries and seasonal variations of the lowermost stratospheric water vapor and ozone derived from SAGE II data, J. Geophys. Res. Atmos., 102(D23), 28177–28184, doi:10.1029/97JD02778, 1997.
Pan, L. L., Hintsa, E. J., Stone, E. M., Weinstock, E. M. and Randel, W. J.: The seasonal cycle of water vapor and saturation vapor mixing ratio in the extratropical lowermost stratosphere, J. Geophys. Res. Atmos., 105(D21), 26519–26530, doi:10.1029/2000JD900401, 2000.
Ploeger, F., Günther, G., Konopka, P., Fueglistaler, S., Müller, R., Hoppe, C., Kunz, A., Spang, R., Grooß, J.-U. and Riese, M.: Horizontal water vapor transport in the lower stratosphere from subtropics to high latitudes during boreal summer, J. Geophys. Res. Atmos., 118(14), 8111–8127, doi:10.1002/jgrd.50636, 2013.
Plumb, R. A.: Stratospheric Transport, J. Meteorol. Soc. Japan. Ser. II, 80(4B), 793–809, doi:10.2151/jmsj.80.793, 2002.
Ramanathan, V. and Carmichael, G.: Global and regional climate changes due to black carbon, Nat. Geosci., 1(4), 221–227, doi:10.1038/ngeo156, 2008.
Ramaswamy, V. and Bowen, M. M.: Effect of changes in radiatively active species upon the lower stratospheric temperatures, J. Geophys. Res., 99(D9), 18909, doi:10.1029/94JD01310, 1994.
Randel, W. and Park, M.: Diagnosing Observed Stratospheric Water Vapor Relationships to the Cold Point Tropical Tropopause, J. Geophys. Res. Atmos., 2019JD030648, doi:10.1029/2019JD030648, 2019.
Revell, L. E., Stenke, A., Rozanov, E., Ball, W., Lossow, S. and Peter, T.: The role of methane in projections of 21st century stratospheric water vapour, Atmos. Chem. Phys., 16(20), 13067–13080, doi:10.5194/acp-16-13067-2016, 2016.
Richardson, T. B., Forster, P. M., Smith, C. J., Maycock, A. C., Wood, T., Andrews, T., Boucher, O., Faluvegi, G., Fläschner, D., Hodnebrog, Ø., Kasoar, M., Kirkevåg, A., Lamarque, J. -F., Mülmenstädt, J., Myhre, G., Olivié, D., Portmann, R. W., Samset, B. H., Shawki, D., Shindell, D., Stier, P., Takemura, T., Voulgarakis, A. and Watson-Parris, D.: Efficacy of Climate Forcings in PDRMIP Models, J. Geophys. Res. Atmos., 124(23), 12824–12844, doi:10.1029/2019JD030581, 2019.

Samset, B. H., Myhre, G., Forster, P. M., Hodnebrog, Ø., Andrews, T., Faluvegi, G., Fläschner, D., Kasoar, M., Kharin, V., Kirkevåg, A., Lamarque, J. -F., Olivié, D., Richardson, T., Shindell, D., Shine, K. P., Takemura, T. and Voulgarakis, A.: Fast and slow precipitation responses to individual climate forcers: A PDRMIP multimodel study, Geophys. Res. Lett., 43(6), 2782–2791, doi:10.1002/2016GL068064, 2016.

Schmidt, G. A., Kelley, M., Nazarenko, L., Ruedy, R., Russell, G. L., Aleinov, I., Bauer, M., Bauer, S. E., Bhat, M. K., Bleck, R., Canuto, V., Chen, Y.-H., Cheng, Y., Clune, T. L., Del Genio, A., de Fainchtein, R., Faluvegi, G., Hansen, J. E., Healy, R. J., Kiang, N. Y., Koch, D., Lacis, A. A., LeGrande, A. N., Lerner, J., Lo, K. K., Matthews, E. E., Menon, S., Miller, R. L., Oinas, V., Oloso, A. O., Perlwitz, J. P., Puma, M. J., Putman, W. M., Rind, D., Romanou, A., Sato, M., Shindell, D. T., Sun, S., Syed, R. A., Tausnev, N., Tsigaridis, K., Unger, N., Voulgarakis, A., Yao, M.-S. and Zhang, J.: Configuration and assessment of the GISS ModelE2 contributions to the CMIP5 archive, J. Adv. Model. Earth Syst., 6(1), 141–184, doi:10.1002/2013MS000265, 2014.

Sherwood, S. C., Bony, S., Boucher, O., Bretherton, C., Forster, P. M., Gregory, J. M. and Stevens, B.: Adjustments in the Forcing-Feedback Framework for Understanding Climate Change, Bull. Am. Meteorol. Soc., 96(2), 217–228, doi:10.1175/BAMS-D-13-00167.1, 2015.

Shu, J., Tian, W., Austin, J., Chipperfield, M. P., Xie, F. and Wang, W.: Effects of sea surface temperature and greenhouse gas changes on the transport between the stratosphere and troposphere, J. Geophys. Res., 116(D2), D02124, doi:10.1029/2010JD014520, 2011.

Smalley, K. M., Dessler, A. E., Bekki, S., Deushi, M., Marchand, M., Morgenstern, O., Plummer, D. A., Shibata, K., Yamashita, Y. and Zeng, G.: Contribution of different processes to changes in tropical lower-stratospheric water vapor in chemistry–climate models, Atmos. Chem. Phys., 17(13), 8031–8044, doi:10.5194/acp-17-8031-2017, 2017.

Smith, C. J., Kramer, R. J., Myhre, G., Forster, P. M., Soden, B. J., Andrews, T., Boucher, O., Faluvegi, G., Fläschner, D., Hodnebrog, Ø., Kasoar, M., Kharin, V., Kirkevåg, A., Lamarque, J. -F., Mülmenstädt, J., Olivié, D., Richardson, T., Samset, B. H., Shindell, D., Stier, P., Takemura, T., Voulgarakis, A. and Watson-Parris, D.: Understanding Rapid Adjustments to Diverse Forcing Agents, Geophys. Res. Lett., 45(21), doi:10.1029/2018GL079826, 2018.

Smith, J. B., Wilmouth, D. M., Bedka, K. M., Bowman, K. P., Homeyer, C. R., Dykema, J. A., Sargent, M. R., Clapp, C. E., Leroy, S. S., Sayres, D. S., Dean-Day, J. M., Paul Bui, T. and Anderson, J. G.: A case study of convectively sourced water vapor observed in the overworld stratosphere over the United States, J. Geophys. Res. Atmos., 122(17), 9529–9554, doi:10.1002/2017JD026831, 2017.

Solomon, S., Garcia, R. R., Rowland, F. S. and Wuebbles, D. J.: On the depletion of Antarctic ozone, Nature, 321(6072), 755–758, doi:doi:10.1038/321755a0, 1986.

Solomon, S., Rosenlof, K. H., Portmann, R. W., Daniel, J. S., Davis, S. M., Sanford, T. J. and Plattner, G.-K.: Contributions of Stratospheric Water Vapor to Decadal Changes in the Rate of Global Warming, Science (80-.)., 327(5970), 1219–1223, doi:10.1126/science.1182488, 2010.

Stjern, C. W., Samset, B. H., Myhre, G., Forster, P. M., Hodnebrog, Ø., Andrews, T., Boucher, O., Faluvegi, G., Iversen, T., Kasoar, M., Kharin, V., Kirkevåg, A., Lamarque, J.-F., Olivié, D., Richardson, T., Shawki, D., Shindell, D., Smith, C. J., Takemura, T. and Voulgarakis, A.: Rapid Adjustments Cause Weak Surface Temperature Response to Increased Black Carbon Concentrations, J. Geophys. Res. Atmos., 122(21), 11,462-11,481, doi:10.1002/2017JD027326, 2017.

Takemura, T., Nozawa, T., Emori, S., Nakajima, T. Y., Nakajima, T.: Simulation of climate response to aerosol direct and indirect effects with aerosol transport-radiation model, J. Geophys. Res., 110(D2), D02202, doi:10.1029/2004JD005029, 2005.

Takemura, T., Egashira, M., Matsuzawa, K., Ichijo, H., O'ishi, R. and Abe-Ouchi, A.: A simulation of the global distribution and radiative forcing of soil dust aerosols at the Last Glacial Maximum, Atmos. Chem. Phys., 9(9), 3061–3073, doi:10.5194/acp-9-3061-2009, 2009.

Tang, T., Shindell, D., Samset, B. H., Boucher, O., Forster, P. M., Hodnebrog, Ø., Myhre, G., Sillmann, J., Voulgarakis, A., Andrews, T., Faluvegi, G., Fläschner, D., Iversen, T., Kasoar, M., Kharin, V., Kirkevåg, A., Lamarque, J.-F., Olivié, D., Richardson, T., Stjern, C. W. and Takemura, T.: Dynamical response of Mediterranean precipitation to greenhouse gases and aerosols, Atmos. Chem. Phys., 18(11), 8439–8452, doi:10.5194/acp-18-8439-2018, 2018.

Tang, T., Shindell, D., Faluvegi, G., Myhre, G., Olivié, D., Voulgarakis, A., Kasoar, M., Andrews, T., Boucher, O., Forster, P. M., Hodnebrog, Ø., Iversen, T., Kirkevåg, A., Lamarque, J. -F., Richardson, T., Samset, B. H., Stjern, C. W., Takemura, T. and Smith, C.: Comparison of Effective Radiative Forcing Calculations Using Multiple Methods, Drivers, and Models, J. Geophys. Res. Atmos., 124(8), 4382–4394, doi:10.1029/2018JD030188, 2019.

Thuburn, J. and Craig, G. C.: On the temperature structure of the tropical substratosphere, J. Geophys. Res., 107(D2), 4017, doi:10.1029/2001JD000448, 2002.

Ueyama, R., Jensen, E. J. and Pfister, L.: Convective Influence on the Humidity and Clouds in the Tropical Tropopause Layer During Boreal Summer, J. Geophys. Res. Atmos., doi:10.1029/2018JD028674, 2018.

Walters, D. N., Williams, K. D., Boutle, I. A., Bushell, A. C., Edwards, J. M., Field, P. R., Lock, A. P., Morcrette, C. J., Stratton, R. A., Wilkinson, J. M., Willett, M. R., Bellouin, N., Bodas-Salcedo, A., Brooks, M. E., Copsey, D., Earnshaw, P. D., Hardiman, S. C., Harris, C. M., Levine, R. C., MacLachlan, C., Manners, J. C., Martin, G. M., Milton, S. F., Palmer, M. D., Roberts, M. J., Rodríguez, J. M., Tennant, W. J. and Vidale, P. L.: The Met Office Unified Model Global Atmosphere 4.0 and JULES Global Land 4.0 configurations, Geosci. Model Dev., 7(1), 361–386, doi:10.5194/gmd-7-361-2014, 2014.

Wang, X., Dessler, A. E., Schoeberl, M. R., Yu, W. and Wang, T.: Impact of convectively lofted ice on the seasonal cycle of water vapor in the tropical tropopause layer, Atmos. Chem. Phys., 19(23), 14621–14636, doi:10.5194/acp-19-14621-2019, 2019.

Watanabe, M., Suzuki, T., O'ishi, R., Komuro, Y., Watanabe, S., Emori, S., Takemura, T., Chikira, M., Ogura, T., Sekiguchi, M., Takata, K., Yamazaki, D., Yokohata, T., Nozawa, T., Hasumi, H., Tatebe, H. and Kimoto, M.: Improved Climate Simulation by MIROC5: Mean States, Variability, and Climate Sensitivity, J. Clim., 23(23), 6312–6335, doi:10.1175/2010JCLI3679.1, 2010.

Xia, Y., Huang, Y., Hu, Y. and Yang, J.: Impacts of tropical tropopause warming on the stratospheric water vapor, Clim. Dyn., 53(5–6), 3409–3418, doi:10.1007/s00382-019-04714-3, 2019.

Zelinka, M. D., T. A. Myers, D. T. McCoy, S. Po-Chedley, P. M. Caldwell, P. Ceppi, S. A. Klein, and K. E. Taylor, 2020: Causes of higher climate sensitivity in CMIP6 models, Geophys. Res. Lett., 47, doi:10.1029/2019GL085782.

Zhang, H.-M., B. Huang, J. Lawrimore, M. Menne, Thomas M. Smith, NOAA Global Surface Temperature Dataset (NOAAGlobalTemp), Version 5.0 [indicate subset used]. NOAA National Centers for Environmental Information. doi:10.7289/V5FN144H [2020-07-13].

Table 1: Description of PDRMIP models (Myhre et al., 2017) and list of perturbation experiments used in this study.

Model	Version	Resolution	Ocean setup	Aerosol setup	Key references	Perturbation experiments
Second Generation Canadian Earth System Model (CanESM2)	2010	2.8°×2.8°, 35 levels	Coupled ocean	Emissions	(Arora et al., 2011)	$2xCO_2$, $3xCH_4$, 2%Solar, 10xBC, $5xSO_4$
Community Earth System Model, version 1 (Community Atmosphere Model, version 4) [CESM1(CAM4)]	1.0.3	2.5°×1.9°, 26 levels	Slab ocean	Fixed concentrations	(Neale et al., 2010; Gent et al., 2011)	$2xCO_2$, $3xCH_4$, 2%Solar, 10xBC, $5xSO_4$, 10xCFC-12, $3xN_2O$, 10xBCSLT
CESM1 CAM5	1.1.2	2.5°×1.9°, 30 levels	Coupled ocean	Emissions	(Hurrell et al., 2013; Kay et al., 2015; Otto-Bliesner et al., 2016)	$2xCO_2$, $3xCH_4$, 2%Solar, 10xBC, $5xSO_4$, 10xCFC-12
Goddard Institute for Space Studies Model E2, coupled with the Russell ocean model (GISS-E2-R)	E2-R	2°×2.5°, 40 levels	Coupled ocean	Fixed concentrations	(Schmidt et al., 2014)	$2xCO_2$, $3xCH_4$, 2%Solar, 10xBC, $5xSO_4$, 10xCFC-12, 10xBCSLT
Hadley Centre Global Environment Model, version 2—Earth System (includes Carbon Cycle configuration with chemistry) (HadGEM2-ES)	6.6.3	1.875°×1.25°, 38 levels	Coupled ocean	Emissions	(Collins et al., 2011; Martin et al., 2011)	$2xCO_2$, $3xCH_4$, 2%Solar, 10xBC, $5xSO_4$, 10xCFC-12, 10xCFC-11, $3xN_2O$

HadGEM3	Global Atmosphere 4.0	1.875°×1.25°, 85 levels	Coupled ocean	Fixed concentrations	(Bellouin et al., 2011; Walters et al., 2014)	$2xCO_2$, $3xCH_4$, 2%Solar, 10xBC, $5xSO_4$, 10xCFC-12
L'Institut Pierre-Simon Laplace Coupled Model, version 5A (IPSL-CM5A)	CMIP5	3.75° ×1.875°, 39 levels	Coupled ocean	Fixed concentrations	(Dufresne et al., 2013)	$2xCO_2$, $3xCH_4$, 2%Solar, 10xBC, $5xSO_4$
Max Planck Institute Earth System Model (MPI-ESM)	1.1.00p2	T63, 47 levels	Coupled ocean	Climatology, year 2000	(Giorgetta et al., 2013)	$2xCO_2$, $3xCH_4$, 2%Solar
Model for Interdisciplinary Research on Climate-Spectral Radiation-Transport Model for Aerosol Species (MIROC-SPRINTARS)	5.9.0	T85 (approx. 1.4°×1.4°), 40 levels	Coupled ocean	Hemispheric Transport Air Pollution, phase 2 Emissions	(Takemura, 2005; Takemura et al., 2009; Watanabe et al., 2010)	$2xCO_2$, $3xCH_4$, 2%Solar, 10xBC, $5xSO_4$, 10xCFC-12, 10xCFC-11, $3xN_2O$, $5xO_3$

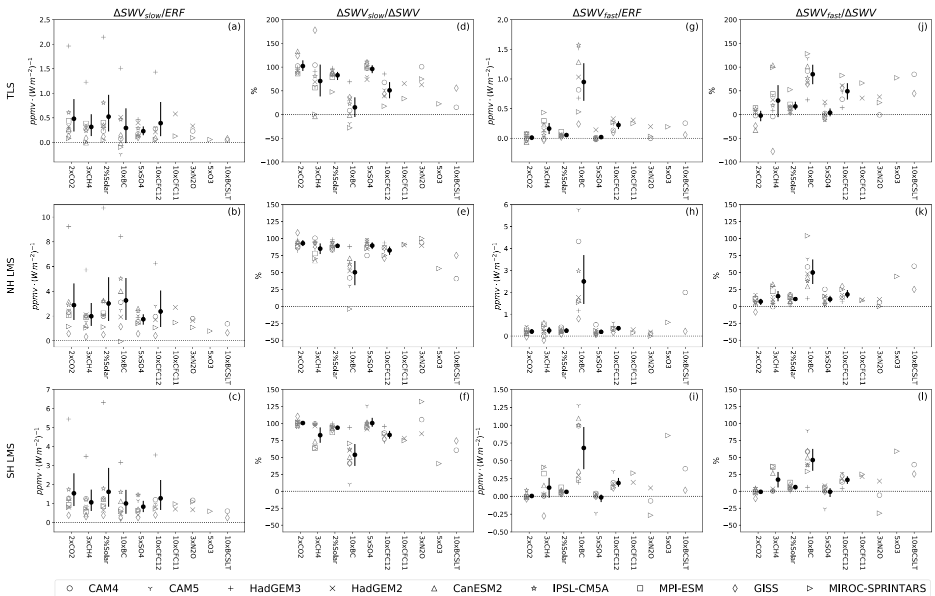

Figure 1. Panels (a)-(c): equilibrium ΔSWV_{slow} normalized by ERF (ppmv·$(Wm^{-2})^{-1}$) in TLS (70 hPa, 30°N-30°S), NH LMS (200 hPa, 50°N-90°N), and SH LMS (200 hPa, 50°S-90°S). Panels (d)-(f): Contribution (%) of equilibrium ΔSWV_{slow} to total equilibrium ΔSWV. Panels (g)-(i): ΔSWV_{fast} normalized by ERF (ppmv·$(Wm^{-2})^{-1}$). Panels (j)-(l): Contribution (%) of ΔSWV_{fast} to total equilibrium ΔSWV. The marker shapes indicate results from different models. For perturbations that are performed by more than three models, the solid circles and error bars for each perturbation plotted in weighted black are multi-model mean and 2.5%-97.5% percentiles of the model samples. Note that in the second and fourth columns, we took out models with extremely small ΔSWV magnitudes that yield extremely large ΔSWV_{slow}/ΔSWV and ΔSWV_{fast}/ΔSWV ratios.

Deleted: The

Deleted: ensemble average

Deleted: confidence interval

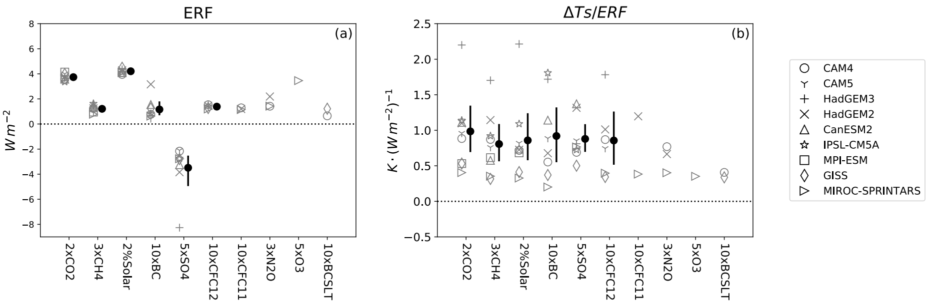

745 **Figure 2. Panel (a): Global average ERF (W m^{-2}) at the top of atmosphere. Panel (b): Global averaged surface temperature change per unit ERF (K·(W m^{-2})$^{-1}$). The marker shapes indicate results from different models. For perturbations that are performed by more than three models, the solid circles and error bars for each perturbation plotted in weighted black are multi-model mean and 2.5%-97.5% percentiles of the model samples.**

Deleted: The

Deleted: ensemble average

Deleted: confidence intervals

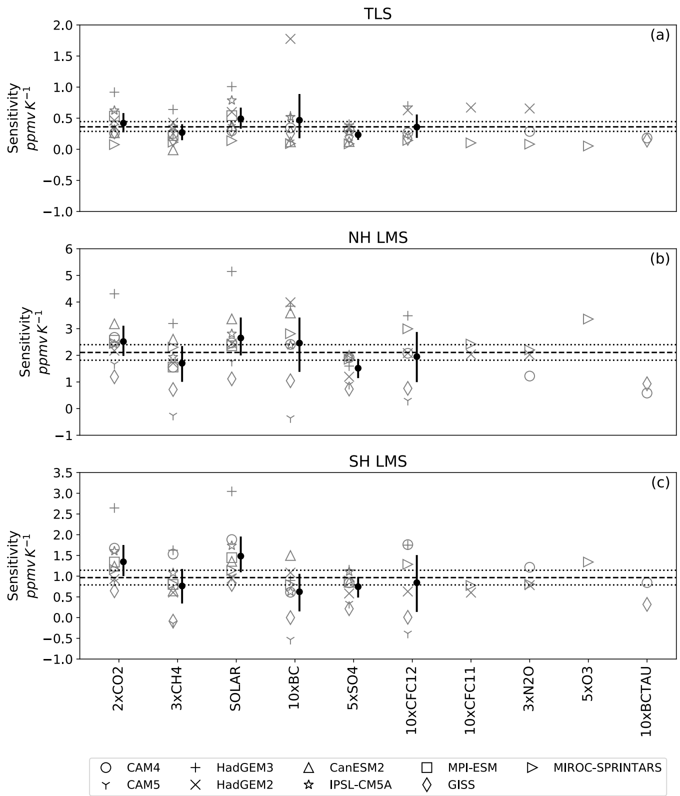

Figure 3. Slopes (ppmv K^{-1}) from the linear regression between annual mean ΔSWV_{slow} time series and annual mean ΔTs time series. The marker shapes indicate results from different models. For perturbations that are performed by more than three models, the solid circles and error bars for each perturbation plotted in weighted black are multi-model mean and 2.5%-97.5% percentiles of the model samples. The horizontal dashed line is the multi-model mean of all slopes, and the horizontal dotted lines are 2.5%-97.5% percentiles of the model samples.

Deleted: The

Deleted: ensemble average

Deleted: confidence intervals.

Deleted: ensemble average

Deleted: confidence intervals

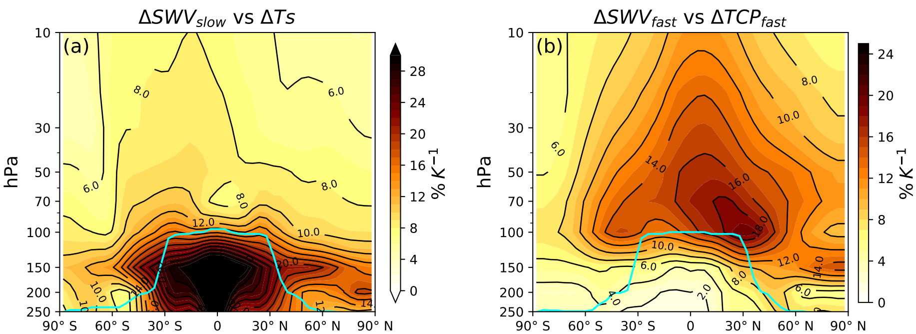

Figure 4. Panel (a): Multi-model and multi-perturbation mean slope (% K[-1]) from the regression between annual mean time series of ΔSWV_{slow} at each latitude grid point and pressure level and annual mean time series of global average ΔTs. Panel (b): Slope (% K[-1]) from the regression between ΔSWV_{fast} (ppmv) at each latitude grid point and pressure level and ΔTCP_{fast} (K). The solid cyan line is the multi-model mean lapse rate tropopause derived from the baseline simulations.

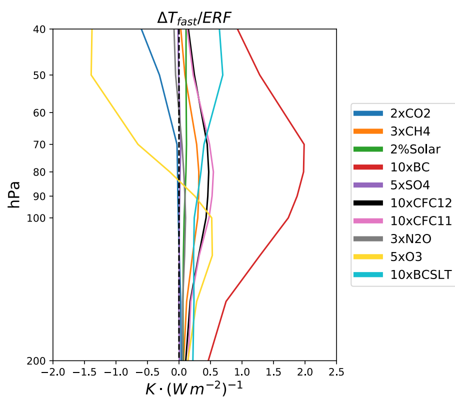

Figure 5. Profiles of fast temperature response normalized by ERF (K·(Wm[-2])[-1]) between 200 and 40 hPa, and averaged over 30°N-30°S. The color coding indicates results from different perturbations. Each profile is the multi-model mean.

Deleted: Ensemble

Deleted: average

Deleted: ensemble average

Deleted: ensemble average

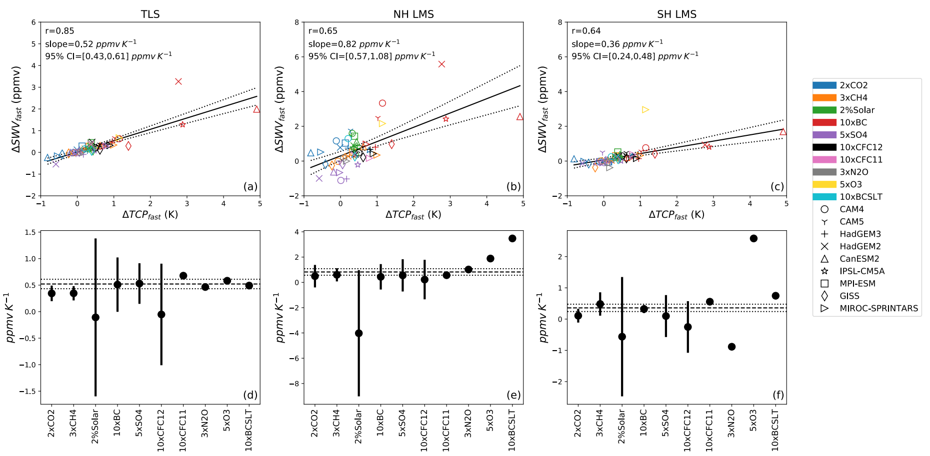

Figure 6. Panels (a)-(c): Linear regression between ΔSWV_{fast} (ppmv) and ΔTCP_{fast} (K) from all models and perturbations. The color coding indicates different perturbations, while the marker shapes indicate results from different models. The black solid line is the linear fit of the regression. The black dotted lines indicate the linear fits within the 95% confidence interval, estimated using a t-test. Panels (d)-(f): Slopes and their 95% confidence intervals (for perturbations that are performed by more than three models) obtained from linear regression between ΔSWV_{fast} (ppmv) and ΔTCP_{fast} (K) for each individual perturbation. The black dashed lines and dotted lines are the slopes and their 95% confidence intervals of regressions in (a)-(c).

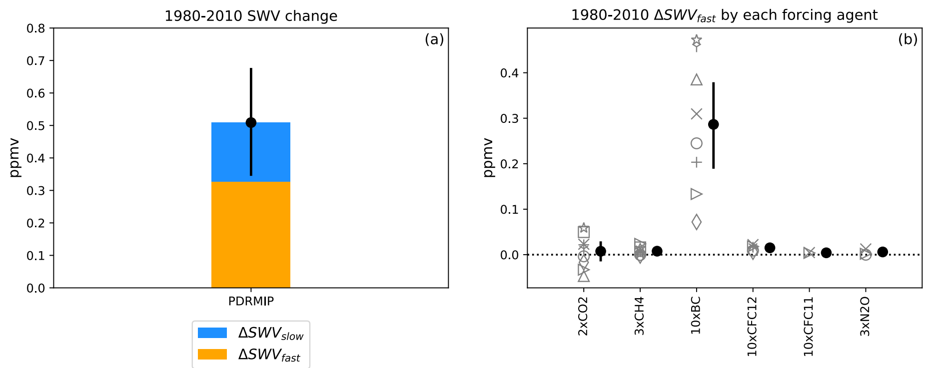

Figure 7. (a) TLS (30°S-30°N, 70 hPa) SWV change over 1980-2010 estimated using PDRMIP results. Blue indicates the component contributed by the slow response, while orange indicates the component contributed by the fast response. (b) The fast component of the PDRMIP-estimated 1980-2010 SWV change contributed by each historical forcing agent. The solid circles are multi-model mean. The error bars are 2.5%-97.5% percentiles of the model samples; in Panel (b) they are shown for perturbations that are performed by more than three models.

Table 2: Historical global average surface temperature change and radiative forcing (RF) by Greenhouse gases (GHGs) and halocarbons over 1980-2010. The SWV change over 1980-2010 estimated using PDRMIP results is also listed, including the total SWV change, the slow component, and the fast component. For the fast component of SWV change contributed by each forcing agent, multi-model mean results are listed. The uncertainties are 2.5%-97.5% percentiles of the model samples.

GMST[a] (K)	0.506
Total ΔSWV (ppmv)	0.51±0.16
ΔSWV_{slow} (ppmv)	0.18±0.04
ΔSWV_{fast} (ppmv)	0.32±0.12

Forcing agents	RF (Wm^{-2})	ΔSWV_{fast} by each forcing agent (ppmv)
CO_2[b]	0.715	0.007±0.022
CH_4[c]	0.055	0.008±0.005
BC[d]	0.3	0.286±0.095
CFC-12[e]	0.068	0.015±0.004
CFC-11[f]	0.015	0.004
N_2O[g]	0.042	0.005

a: We used NOAA Merged Land Ocean Global Surface Temperature Analysis V5 (Zhang et al. 2020) to compute the global surface temperature change. We use values averaged over 2005-2015 minus that averaged over 1975-1985.
b, c, e, f, and g: We compute the RFs using the formulae listed in Table 3 of Myhre et al. (1998). These formulae were also used to compute RFs of CO_2, CH_4, and N_2O in IPCC reports (Myhre et al. 2013).
b, c, and g: Concentrations of GHGs were used to compute RFs. CO_2 and CH_4 are samples collected in glass flasks at Cold Bay, Alaska, United States (CBA) from the ERSL GML website (Dlugokencky et al. 2020). N_2O is from the Combined Nitrous Oxide data from the NOAA/ESRL Global Monitoring Division. For CO_2, concentrations averaged over 2005-2015

and averaged over 1978-1985 are used. For CH_4, concentrations averaged over 2005-2015 and averaged over 1983-1985 are used. For N_2O, concentration averaged over 2005-2015 and averaged over 1977-1985 are used.

e-f: Concentrations of CFC-12 and CFC-11 were used to compute RFs. We use CFC-12 and CFC-11 data from combined stations from the NOAA/ESRL Global Monitoring Division. Concentrations averaged over 2005-2015 and averaged over 1977-1985 are used.

d: We use 0.4 Wm^{-2}, the BC RF between 1750-2011 reported in IPCC AR5, minus 0.1 Wm^{-2}, the BC RF between 1750-1993 reported in 1995 IPCC report (See Table 8.4 of Myhre et al. 2013).